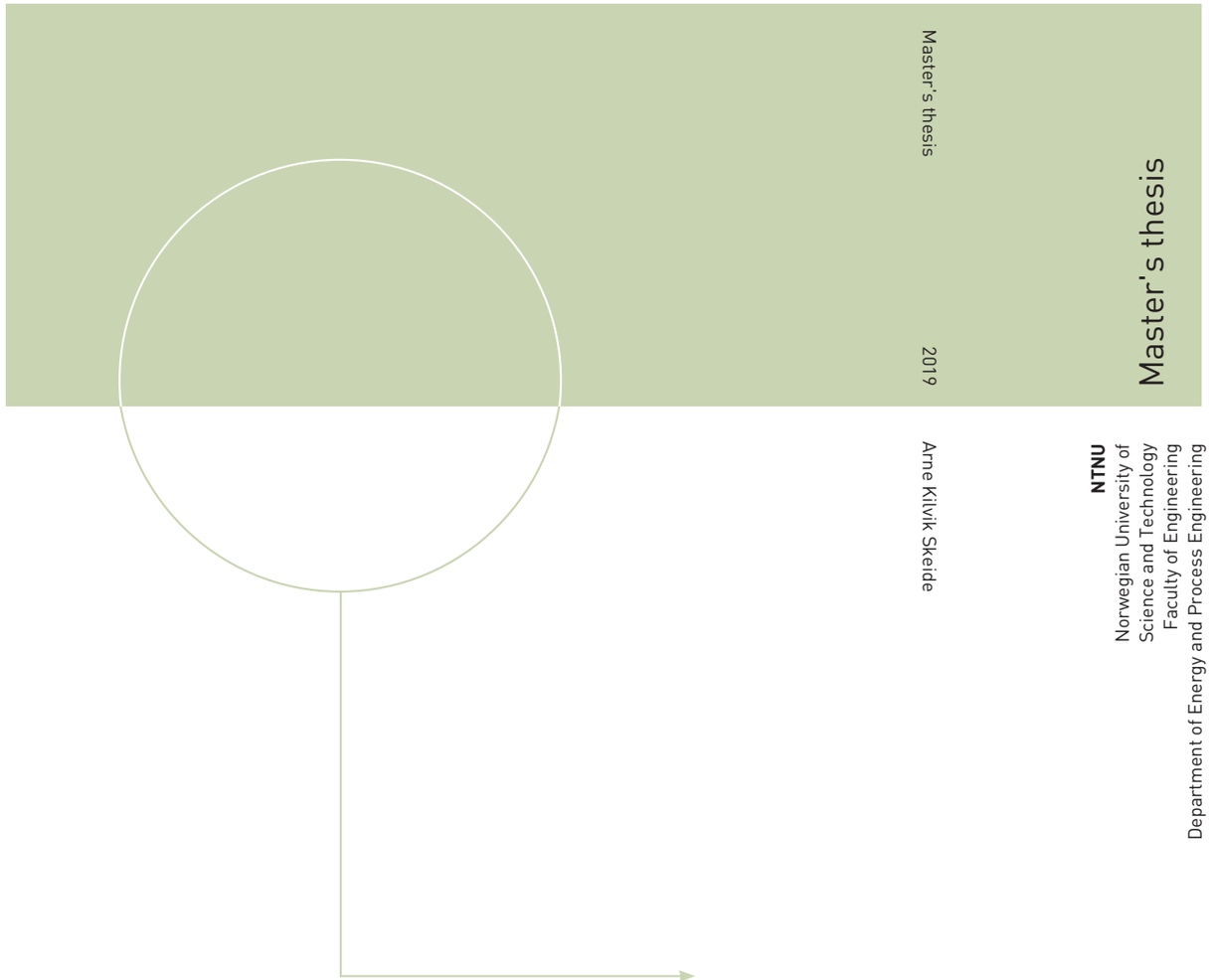

Master's thesis

2019

Arne Kilvik Skeide

NTNU
Norwegian University of
Science and Technology
Faculty of Engineering
Department of Energy and Process Engineering

Arne Kilvik Skeide

Significant Drag Savings on a Cylinder using Ribs and Textiles

June 2019

NTNU
Norwegian University of
Science and Technology

NTNU
Norwegian University of
Science and Technology

NTNU
Norwegian University of
Science and Technology

Significant Drag Savings on a Cylinder using Ribs and Textiles

Arne Kilvik Skeide

Mechanical Engineering
Submission date: June 2019
Supervisor: Robert Jason Hearst
Co-supervisor: Lars Morten Bardal and Luca Oggiano

Norwegian University of Science and Technology
Department of Energy and Process Engineering

Abstract

The impact of ribs and small-scale surface roughness on the drag and vortex shedding of a circular cylinder is investigated herein. The cylinder was covered by a 'textile' which consisted of semicircular ribs perpendicular to the flow that were covered by one of three different fabrics. The textiles' ribs were equally distributed and had equal shape and size. Three rib heights, four relative rib spacings (spacing/height) and three coating fabrics, were combined to produce 28 unique textiles with different surface structures. The surface structures were analysed by scanning the surfaces with a 3D-scanner. The drag force on the cylinder covered by the different textiles was measured in a wind tunnel for Reynolds numbers in the range $20,000 < Re < 160,000$, representing nearly a decade change centred about the drag crisis. Velocity measurements at a point in the wake of the cylinder were performed with hot-wire anemometry to comment on changes to the shedding frequency.

The results show significant average drag reduction, up to 38%, for most of the rib geometries compared to a smooth cylinder. Increasing rib height caused the critical Reynolds number to decrease and the minimum drag coefficient to increase. It also caused the peak in the Strouhal number in the wake to decrease at the critical Reynolds number. Varying the rib spacing resulted in one "optimal" rib spacing, being five times the rib height, that caused the lowest critical Reynolds number, with larger rib spacings resulting in a strong dependence on the incoming flow angle, and smaller spacings resembling the smooth case with a higher critical Reynolds number. Increasing the micro-roughness, by changing the coating fabric, resulted in a decrease in the critical Reynolds number and an increase in the minimum drag coefficient, supercritical slope and transcritical drag coefficient.

The critical Reynolds number and the minimum drag coefficient for each textile were correlated with their respective surface structures by the use of surface parameters. These parameters were estimated from the two-dimensional fast Fourier transform of the surface scan made for each textile. Polynomial fits were fit to the critical Reynolds number versus one surface parameter and for the minimum drag coefficient versus a different surface parameter. Each fit showed global trends, and the minimum drag coefficient was modelled with a standard deviation below 9% within the measured Re-domain.

Sammendrag

Effekten av striper og små-skala overflateruhet på luftmotstanden og virvelavløsningen til en sirkulær sylinder, har blitt undersøkt. En sylinder ble dekket av et 'tekstil' bestående av halvsirkulære striper liggende vinkelrett med strømningsretningen, med et av tre forskjellige stoff laminert utenpå. Tekstilets striper var likt fordelt og hadde lik form og størrelse. Tre stripehøyder, fire relative avstander (avstand/høyde) og tre stoff med ulik ruhet ble kombinert til 28 unike tekstiler med ulike overflatestrukturer. Overflatestrukturene ble analysert ved å skanne overflatene med en 3D-skanner. Luftmotstanden på sylinderen dekket av de forskjellige tekstilene ble målt i en vindtunnel for Reynoldstall i området $20,000 < Re < 160,000$, som representerer nesten en tierpotens endring sentrert rundt "dragkrisen". Hastighetsmålinger på et punkt i vaken nedstrøms for sylinderen, ble utført ved bruk av varmetrådsanemometri for å se på endringer i virvelfrekvensen.

Resultatene viste betydelige reduksjoner i gjennomsnittlig luftmotstand for de fleste tekstiler, sammenlignet med en glatt sylinder, med verdier opp til 38.1%. Økende stripehøyde førte til lavere kritisk Reynoldstall og høyere minimal luftmotstandskoeffisient. Det førte også til at toppen i Strouhaltallet ble redusert ved det kritiske Reynoldstallet. Variasjoner i stripeavstanden resulterte i en "optimal" avstand som var fem ganger stripehøyden, som forårsaket det laveste kritiske Reynoldstallet, hvor økende stripeavstander forårsaket ueffektive geometrier som var svært avhengige av retningen på luftstrømmen, og hvor synkende stripeavstander skapte en glatningseffekt med høyere kritiske Reynoldstall. Ved å bruke stoff med høyere mikroruhet ble det kritiske Reynoldstallet redusert, og den minimale luftmotstandskoeffisienten, den superkritiske helningen og den transkritiske luftmotstandskoeffisienten, ble økt.

Det kritiske Reynoldstallet og den minimale luftmotstandskoeffisienten for hvert tekstil ble korrelert med de respektive overflatestrukturene ved bruken av overflateparametere. Disse parameterene ble for hvert tekstil hentet fra verdier i den to-dimensjonale Fouriertransformasjonen av overflateskanningen. Polynomiske tilpasninger ble gjort for det kritiske Reynoldstallet som funksjon av en overflateparameter, og for den minimale luftmotstandkoeffisienten som funksjon av en annen overflateparameter. Begge de polynomiske tilpasningene viste globale trender, og den minimale luftmotstandskoeffisienten ble modellert med et standardavvik på under 9% innen det målte Re-området.

Preface

The problem studied in this work was presented to me by Luca Oggiano, Lars Morten Bardal and Ola Elfmark in Centre for Sports Facilities and Technology, based on their current research on sports garments. I would like to extend my gratitude to them for trusting me with such an interesting problem, and to Luca and Lars Morten for also co-supervising my work with indispensable guidance. I must also give a large thanks to my supervisor Robert Jason Hearst, your enthusiasm, availability, guidance and many inputs have meant a million for my work. Thanks also for letting me join your fluid dynamics group during this period. I learned a lot from that experience and would like to also thank the group members. Thanks to Leon Li for also helping out with the hot-wire measurements.

Arne Kilvik Skeide

Trondheim, June 2019

Contents

Chapter 1

Introduction

The flow around circular cylinders and the resulting forces have been studied extensively over the last century. This is due to the fact that the applications are far-reaching. Flow around circular cylinders can for instance be found on oil platforms, wind turbines, tall buildings and in sports aerodynamics. These are applications where the resulting forces have large impacts, and are ideally reduced as much as possible. It is therefore crucial to find ways to reduce these forces. It is still a challenge in fluid dynamics to be able to explain, and calculate, the variations in the non-dimensionalised drag force, known as the drag coefficient,

$$C_D = \frac{F_D}{\frac{1}{2}\rho U^2 A}, \tag{1.1}$$

where U is the free-stream velocity, A is the frontal area and F_D is the drag force [1]. The drag force consists of skin friction drag and pressure drag, where the skin friction is due to the viscous friction between the surface of the cylinder and the surrounding fluid, while the pressure drag is due to flow separation, and is often called form drag. For cylinders, the pressure drag is the dominating part of the total drag.

As a first order approximation it can be stated that C_D is a function of the shape, the motion and the surface of the cylinder [2], $C_D = f$(shape, motion, surface). The shape and motion are dependent on the form of the cylinder and the Reynolds number,

$$Re = \frac{Ud}{\nu}, \tag{1.2}$$

where d is the characteristic length, chosen to be the diameter for spheres and cylinders, and ν is the kinematic viscosity of the fluid. The Re can be defined as the ratio between inertial and viscous forces. At low Re, viscous forces are dominant and the flow is laminar. Laminar flows are characterised by smooth, constant fluid motion. At high Re, inertial forces are the dominant forces and the flow becomes turbulent.

The change in C_D for a circular cylinder by varying Re, known as the C_D-Re curve, has been studied by many authors across a wide Re-domain and is well-documented. Schewe [3] and Achenbach [4], among others, have shown that the C_D-Re curve consists of four flow ranges: the subcritical, critical, supercritical and transcritical range. Achenbach [4] also showed that by changing the surface roughness the trajectory of the C_D-Re curve changed. Changing the surface roughness yields a different critical Reynolds number, Re_c, defined as the Re at the end of the critical flow range, a different minimum C_D, $C_{D,m}$, defined as the minimum C_D-value on the curve, and a different transcritical C_D, $C_{D,t}$, which is the roughly constant C_D reached at the largest Re after having increased from $C_{D,m}$ through the supercritical flow range. Schewe [3] analysed the

drag on a smooth cylinder and found the subcritical C_D, $C_{D,s}$, to be between 1.1 and 1.2, Re_c to be approximately 300,000, $C_{D,m}$ to be approximately 0.2, and a $C_{D,t}$ at about 0.6. This means that a smooth cylinder will experience a sharp decrease in drag for $Re > 300,000$. This sharp decrease in drag is desirable, but many applications have Re well below this. For instance, a cyclists upper arm, if modelled as a cylinder, would experience air flows at $25,000 < Re < 100,000$.

Many methods have been used to describe surface structures in simplified models. The idea behind creating these models is that the drag force on any surface can be calculated by simply scanning and analyzing the surface. This removes the need for measuring forces on surfaces in expensive experimental setups. Achenbach [4] used the relative roughness model to describe the surface topology, which is a common approach. This model says that the friction drag on a cylinder depends on Re and the relative roughness k_s/d, which is the ratio of the mean height of roughness of the cylinder to the cylinder diameter. The results are obtained from experiments using artificially roughened surfaces (usually by gluing sand grains of a known size onto the cylinder) [1]. The surface of the cylinder with unknown drag are then scanned to find the relative roughness k_s/d, and compared to experiments of an artificially roughened surface with the same k_s/d, to find the equivalent drag. This is equivalent to using the Moody diagram for pipe flows [1]. This method is however an unsatisfactory way to describe surface topographies since it lacks information about the scale of the roughness [2]. This would mean that for each measured relative roughness k_s/d, there is almost an endless amount of roughness scales that would give the same k_s/d, but different trajectories of the C_D-Re curve. An example of this was shown by Bearman & Harvey [5] using dimples on a cylinder.

Signifcant research has therefore been done on engineering surface structures which could manipulate the flow around bodies, causing the lowest possible drag forces in a given Re-domain. Because drag reduction is closely related to energy savings, the applications are far-reaching. One of these applications is the engineering of textiles for use in sports garments. Reducing the skin friction drag has a large impact on the performance of athletes. Brownlie [6] showed that athletes can be modelled as a system of bluff bodies, arms and legs as cylinders of different diameters for instance. This means that different surface structures are needed on the different body parts to be able to minimize the drag.

Reducing the drag force on a body can be done using flow control techniques. Flow control techniques can often be categorized into two types, active and passive. Active control requires a certain energy input, for instance suction, while passive control only requires a change of the body or surface [7]. A change in the surface could be referred to as adding a ”macro-roughness” to the surface’s ”micro-roughness” structure. Passive flow control techniques are often simpler and cheaper to implement in engineering applications due to their low level of complexity relative to active flow control. Many different methods have been explored for using passive flow control on different bodies. Raayai-Ardakani & McKinley [8], inspired by the design of the ribbed structure of shark skin, explored the effects of periodic sinusoidal riblet surfaces aligned in the flow direction on a flat plate. The concept of using riblets was first introduced in 1979 by Walsh & Weinstein [9], and has later been examined extensively. The use of riblet surfaces have also been used on cylinders. Ko, Leung & Chen [10] explored the effect that streamwise riblets would have on the drag and the wake structure when fitted onto a cylinder. Lim & Lee [7] explored the difference in drag and wake structure between streamwise U- and V-grooved surfaces.

Other passive control techniques tested on circular cylinders include surface roughness (Achenbach [4], Nakamura & Tomonari [11]), dimples (Bearman & Harvey [5]), grooves (Kimura & Tsutahara [12], Yamagishi & Oki [13] [14]), span-wise waviness (Ahmed & Bays-Muchmore [15], Lam & Lin [16]), helix (Zhou et al. [17], Lee & Kim [18]), wake splitter plates (Hwang & Yang [19]), and spanwise ribs (Zhang et al. [20], Matsumura et al. [21], Zdravkovich [22]). Some of these control methods, including surface roughness, dimples, grooves and spanwise ribs, are

changing the cross-sectional shape or surface structures of the cylinder. The idea behind these methods is to induce turbulence in the shear-layer, thereby increasing the momentum of the flow, causing the flow to overcome the adverse pressure gradient and delay the separation from the cylinder. This would trigger the drag crisis and result in a narrower wake and a smaller drag coefficient.

An open question is how the aerodynamic properties (e.g., Re_c, $C_{d,m}$) change with the different rib geometries. Matsumara et al. [21] tested three different cylinders with different numbers of equally distributed triangular ribs. They showed a tendency of lower Re_c with larger frequency of ribs, but more than three test cases would be needed to show a clear trend. The base of the ribs are also connected in the three cases, giving ribs of different shapes. It would be interesting to test the effect of ribs of equal shape, but different sizes and spacings between them. Zhang et al. [20] did a numerical analysis on sinusoidal ribs, but only on one rib geometry and only on one subcritical Re. Semi-circular ribs could theoretically be a preferred choice due to circular bodies in general having a lower C_D than bodies with sharp edges. Another question is how does micro roughness impact the effects of the primary macro-scale ribs? In particular, there is little detailed research describing what happens when both macro-scale riblets and micro-scale roughness are used at the same time. The relative roughness model is not sufficient to estimate the aerodynamic properties of this type of the multi-scale ribbed surface structure. A better approach might be to characterize the surface by a roughness spectrum, showing the peaks at the various length scales.

The goal of this work is to test the aerodynamic properties of flow-normal, equally distributed, semi-circular ribs on a cylinder covered by micro-roughness, and correlate these to the parameters of the surface topology. The size and spacings of these ribs was varied along with variations of the surface coating's micro roughness.

Chapter 2

Experimental Setup

2.1 Test cases

Textiles with varied micro- and macro-surface topologies were fit to a 417 mm long cylinder with 75 mm diameter. Force measurements, hot-wire measurements and surface scans were performed on these cylinders. The diameter of the test cylinder was chosen to achieve Re that would capture the drag crisis for all surface coatings, hereafter referred to simply as 'textiles'. The textiles consisted of two layers of fabric with 3D-printed ribs laminated in between the two layers. The ribs had semicircular cross-sections, as illustrated in figure 2.1. Here, θ_1 is the angle between the front of the cylinder and the last rib. The value for θ_1 varied between 150 and 160 degrees. A region without ribs was left on the downstream side of the cylinder as a result of the manufacturing process. However, it was verified that separation always occurred before the last rib, and thus the impact of not having ribs $\pm 30^\circ$ of the rear of the cylinder was minimal.

The textiles were varied using three variables: the height of the ribs' cross-sections divided by the cylinder diameter, the relative spacing between the ribs given as the distance between the edges of the neighbouring ribs divided by their height, and the choice of coating fabric. The different coating fabrics consisted of threads of different materials and had different weaves. The maximum roughness height was measured from surface scans to be 0.10 mm for coating fabric A, 0.20 mm for coating fabric B and 0.42 mm for coating fabric C.

The different parameters described in table 2.1 were combined into 28 unique surface coating textiles for the cylinder. A naming convention for each textile was chosen to be S_a, h_b, Δ_c, where a, b and c are the coating fabric, rib height and rib spacing, respectively. While theoretically more combinations were possible, it was found that certain configurations either did not yield substantially different results or were too difficult to manufacture. Nonetheless, the present investigation still represents the largest and most detailed parameter space explored for surface coating on a circular cylinder.

Table 2.1: The parameters for variations in rib geometry and surface micro roughness.

Textile parameters				
Rib height, h	0.5 mm	1.0 mm	2.0 mm	
Relative rib spacing, Δ/h	2.5	5	10	20
Relative rib height, h/d	0.0067	0.0133	0.0267	
Coating fabric, S	A	B	C	

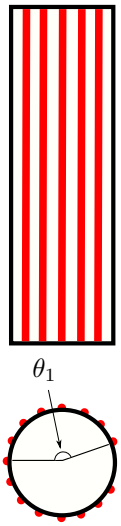

Figure 2.1: Schematic of cylinder rib structure.

2.2 Surface scanning

Each textile was in turn put onto a flat plate with the same perimeter as the test cylinder, and placed on a FESTO linear traverse underneath a MicroCAD premium surface scanner. A 73 mm $\times$ 10 mm scan (9119 $\times$ 1236 pixels) of each textile surface, with the longer side going across the ribs, was then conducted. An example of a scan can be seen in figure 2.2. The scans were then analysed using two-dimensional fast Fourier transform. This gave surface spectra for each textile, showing the peaks at the different roughness scales. Examples of these surface spectra are shown in figures 2.3, 2.4 and 2.5.

2.3 Drag force measurements

The textiles were put onto the 417 mm long, 75 mm diameter test cylinder, which in turn was placed inside a closed-circuit wind tunnel at the Fluid Mechanics Lab at NTNU. The wind tunnel test section has a 1000 mm $\times$ 520 mm cross-section. Two approximately 48 mm long dummy-cylinders of 75 mm in diameter were placed alongside the test cylinder, one above and one below with approximately 3 mm gaps to the test cylinder. This was done to prevent boundary layer effects. The aspect ratio in this case became relatively low (5.56), but most applications actually have finite length cylinders and attempts were made to remove the end effects by the use of the dummy cylinders. The test cylinder was connected to two AMTI MC3A-100 force sensors through a steel rod, one 350 mm above the upper wind tunnel wall and one 170 mm below the lower wind tunnel wall. The sensors were each connected to an AMTI GEN5 Smart Amp load cell amplifier, which in turn were connected to a computer running LabView. The drift in the signal was measured and calculated to be less then 1%. The wind tunnel setup is illustrated in figures 2.6a and 2.6b.

Dynamic measurements of the drag force were done for each textile. Starting at $Re = 20,000$, the velocity was increased steadily to approximately $Re = 160,000$ over a period of 4 minutes, while measuring at a frequency of 1000 Hz. This was repeated five times, giving five C_D-Re curves, for each textile. These five curves were then averaged to yield a smooth and continuous curve for each textile. The averaged curves for all test cases are gathered in figure 2.7, and are broken down in the following sections. Static force measurements at constant Re were also

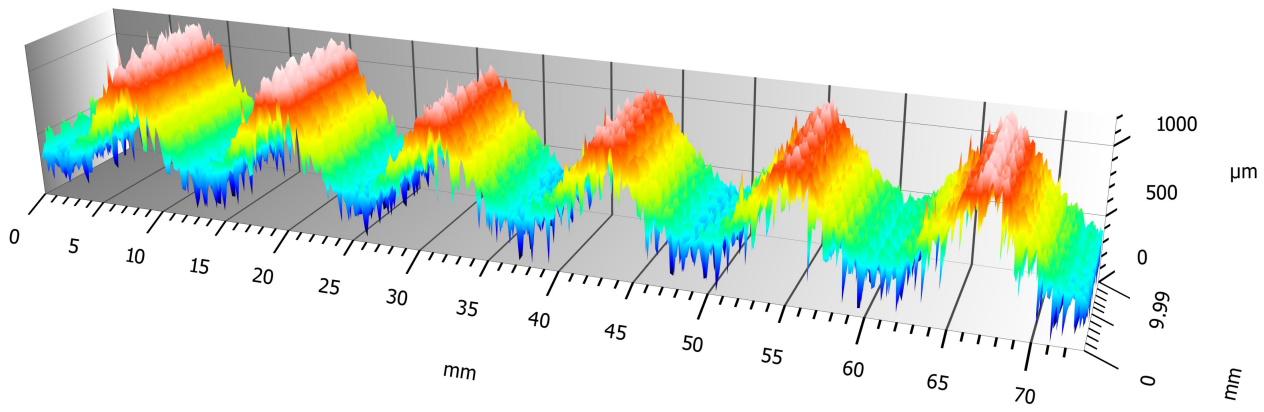

Figure 2.2: 3D-view of the surface scan for textile S_C, h_1, Δ_{10}.

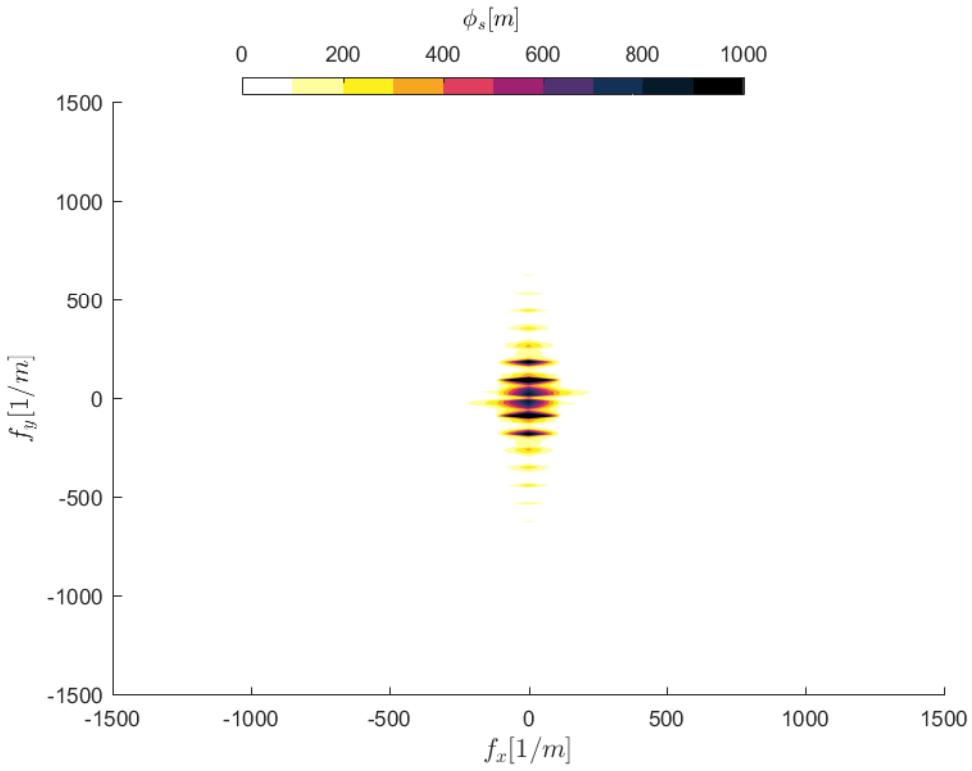

Figure 2.3: 2D FFT for $S_A, h_{0.5}, \Delta_{10}$. A is the smoothest coating and thus doesn't show off-axis energy.

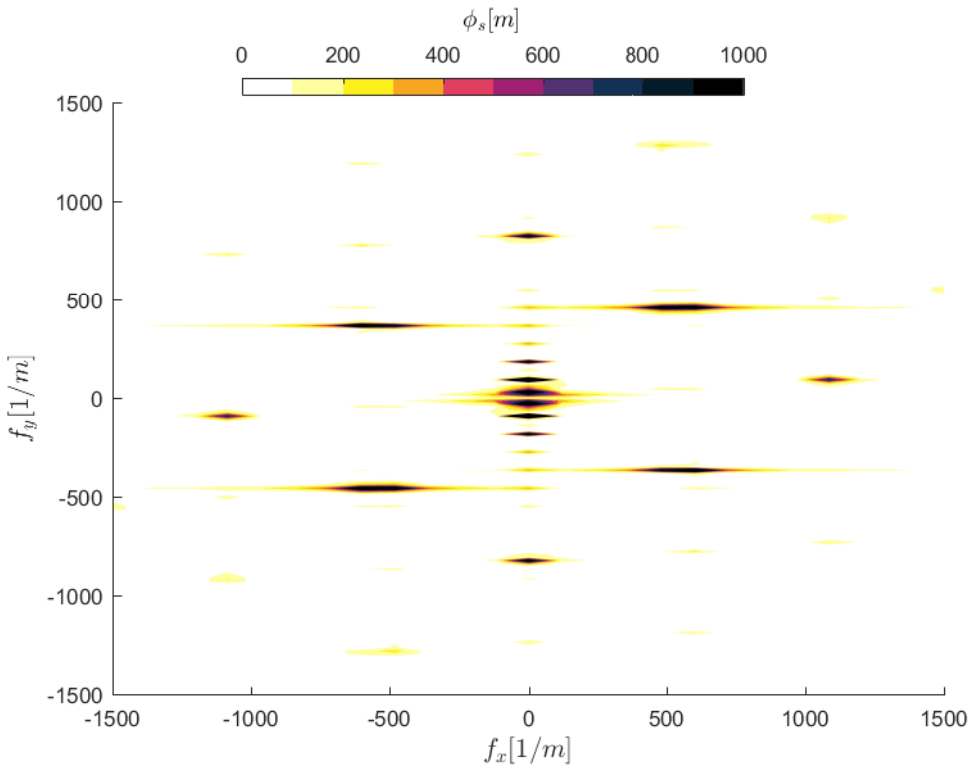

Figure 2.4: 2D FFT for $S_C, h_{0.5}, \Delta_{10}$. C is the roughest coating showing micro-roughness effects.

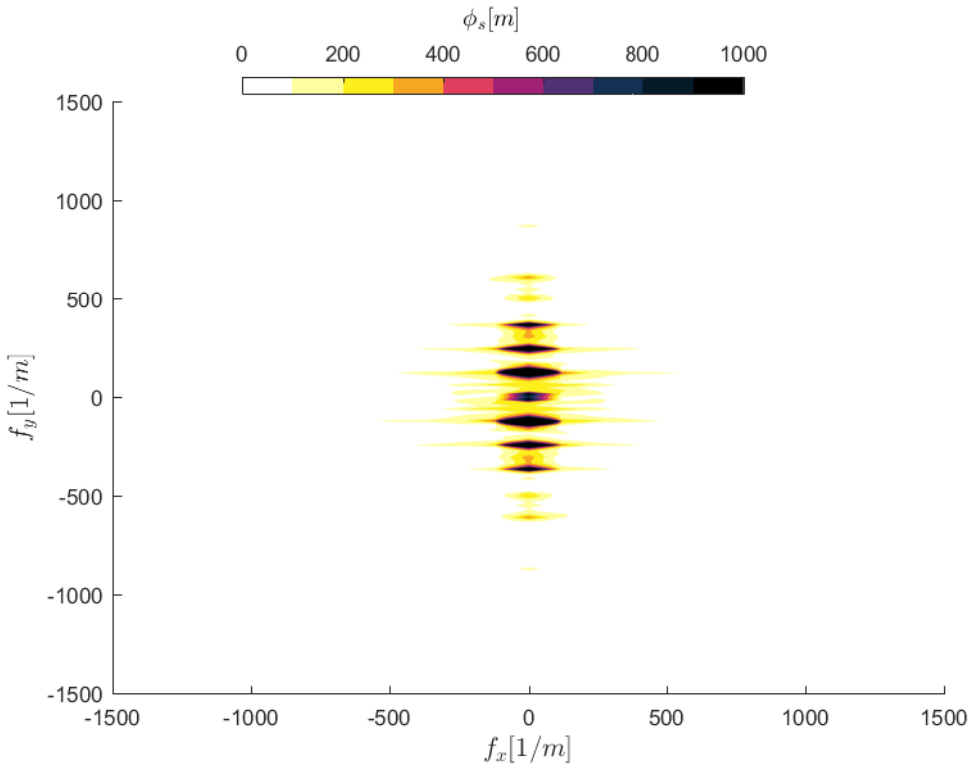

Figure 2.5: 2D FFT for S_A, h_2, Δ_5. Larger rib size gives more energy to the largest peak.

done for some of the textiles, to verify that the dynamic measurement method gave an accurate curve. Figure 2.8 shows the C_D-Re curve for the averaged curve and static measurements for one of the textiles.

2.4 Hot-wire anemometry

Velocity measurements in the wake of the cylinder were conducted in a separate experiment with a single-wire hot-wire (Dantec type 55P11) placed $4.9d$ downstream from the cylinder axis, $0.7d$ off the centerline and along the zero axis. This position was chosen based on previous work of Roshko [23]. The wires were operated in constant temperature mode with an overheat of α = 1.8 using a Dantec Streamline Pro anemometer. A pitot-static tube was placed 100 mm above and 20 mm downstream of the hot-wire, and a Dantec resistance temperature detector (RTD) probe was placed 20 mm above and 150 mm downstream of the hot-wire. Another pitot-static tube was placed 2 m upstream of the cylinder axis and at the centerline. The downstream pitot-static tube was used for the calibration of the hot-wire, while the upstream pitot-static tube measured the free-stream velocity. These were connected to a pressure transducer, and all signals were acquired using a National Instruments NI cDAQ-9174 (DAQ). The hot-wire and temperature outputs from the anemometer along with the pressure transducer were connected to an NI 9215 module in the DAQ.

The hot-wire was calibrated with 11 velocities fit with a fourth-order polynomial. Pre- and post-calibrations were performed at the start and end of each day of measurements to account for hot-wire drift. To correct for temperature drift, the temperature correction methodology of Hultmark & Smits [24] was employed. To assess the shedding phenomena in the wake of the

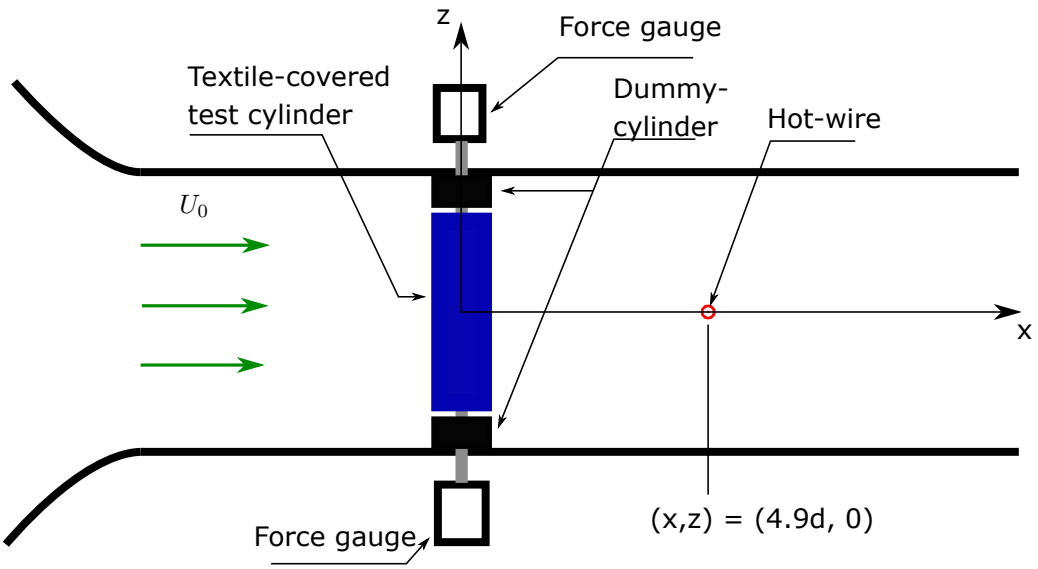

(a) Side view of wind tunnel setup.

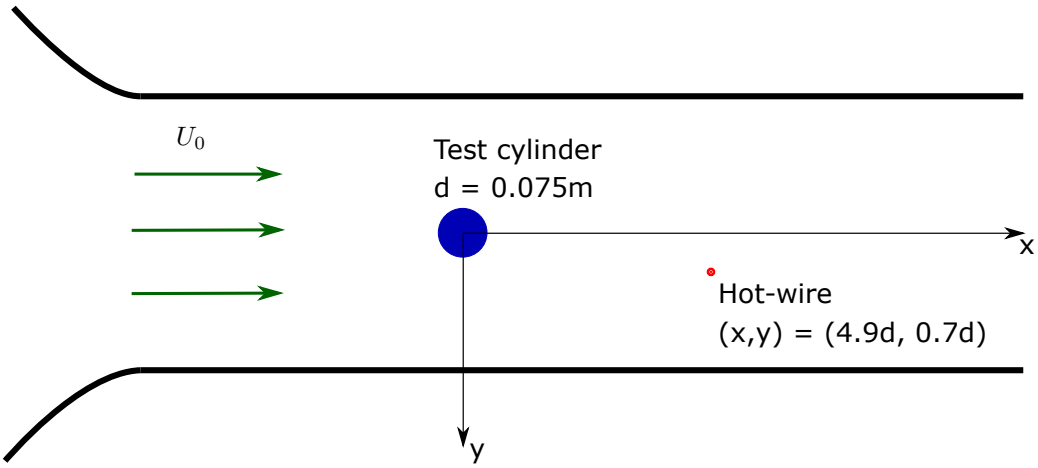

(b) Top view of wind tunnel setup.

Figure 2.6: Wind tunnel setup including position for the hot-wire.

cylinder, six velocities were sampled for each textile. The sampling time was 4 min for all cases, with a sample frequency of 75 kHz. The analog cut-off filter was 30 kHz. Turbulence spectra for two of the cases are shown in figures 2.9 and 2.10. The Strouhal-numbers, defined as

$$St = \frac{fd}{U_0} \tag{2.1}$$

where f is the shedding frequency, were drawn from the spectra using the frequency from the distinct vortex shedding peaks.

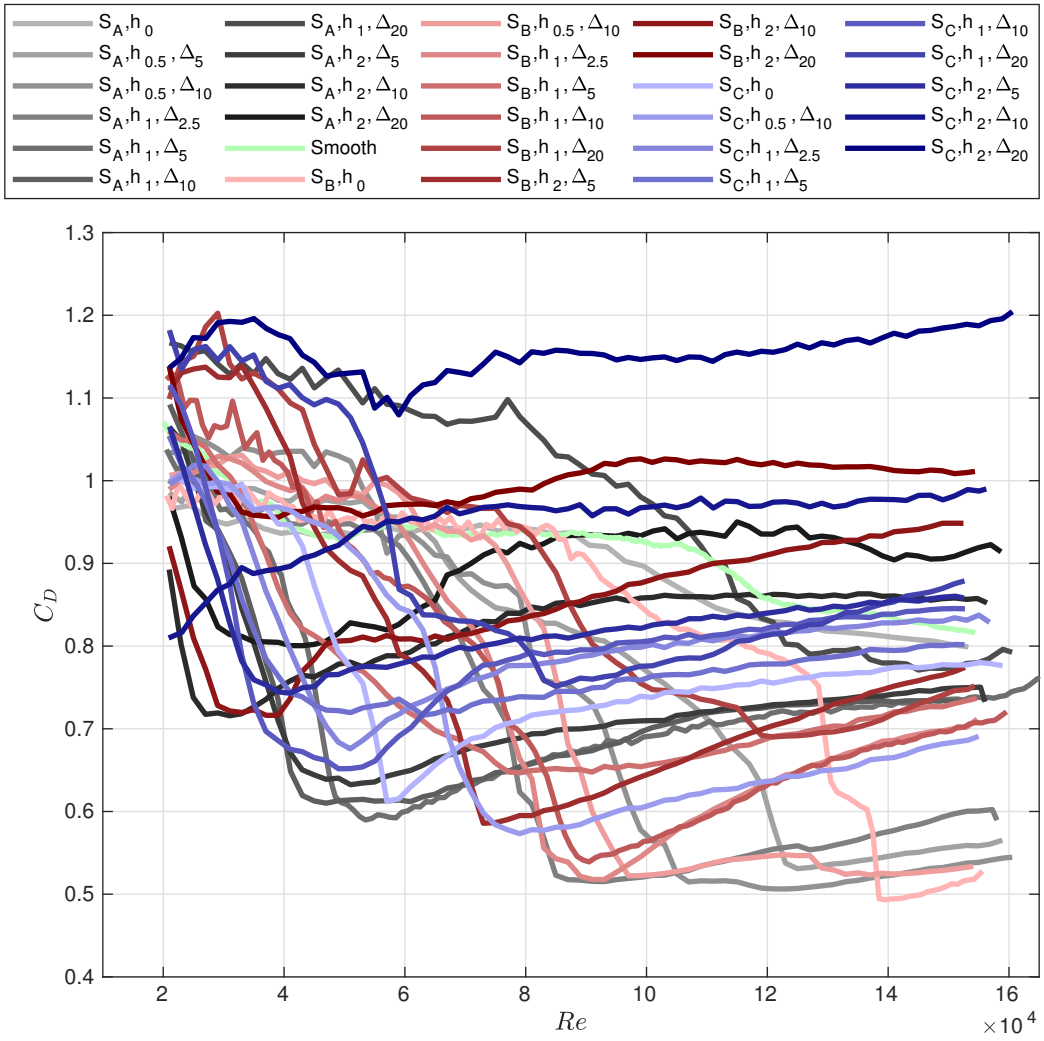

Figure 2.7: Cd-Re curves for all test cases.

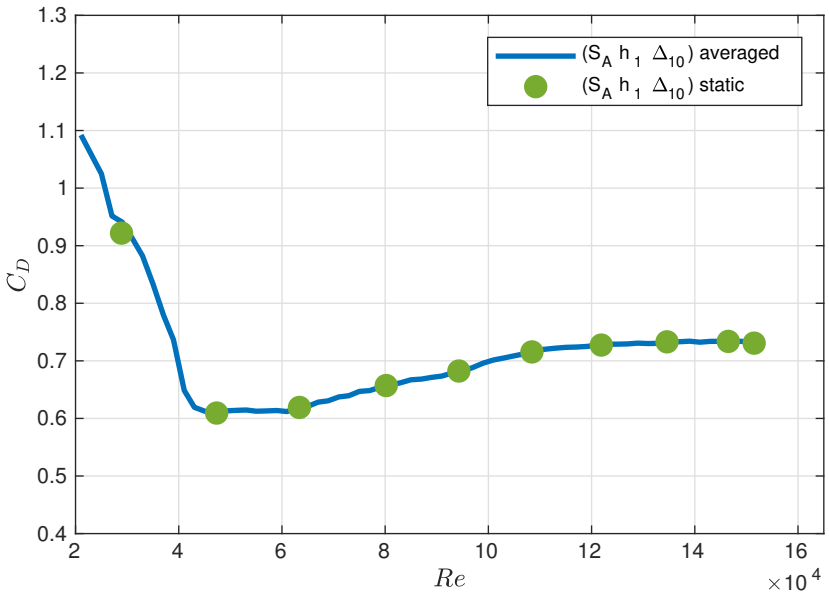

Figure 2.8: Comparing the averaged dynamic drag measurements to the static drag measurements for S_A, h_1, Δ_{10}.

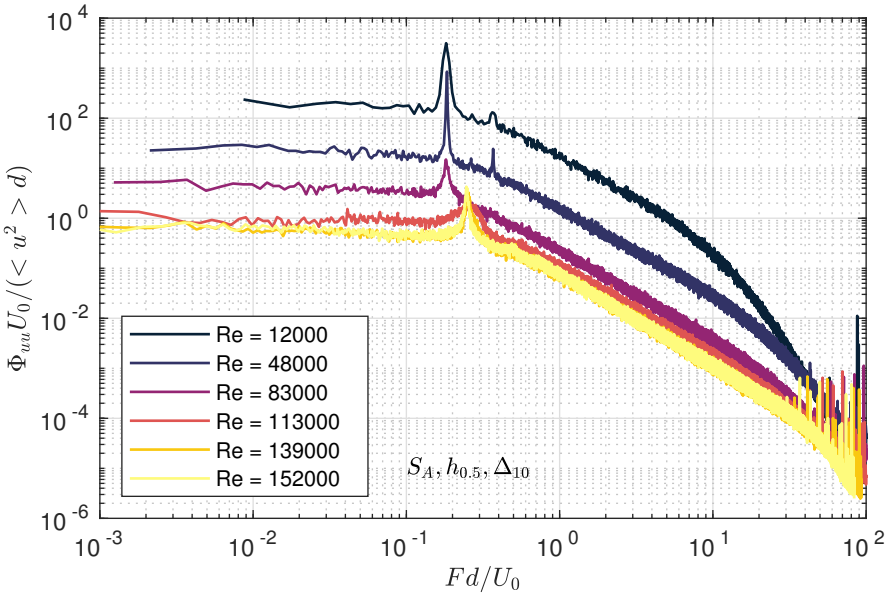

Figure 2.9: Turbulence spectra for textile $S_A, h_{0.5}, \Delta_{10}$.

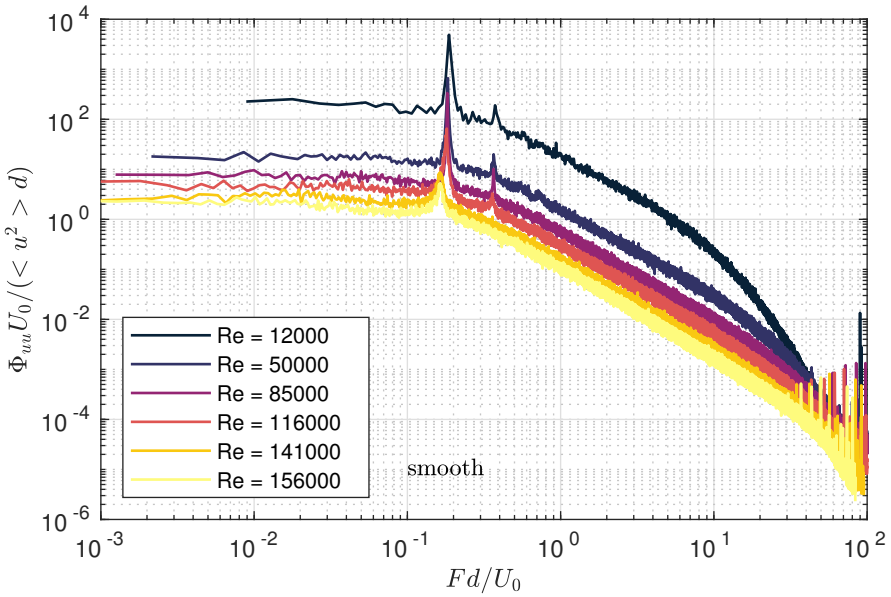

Figure 2.10: Turbulence spectra for the smooth cylinder.

Chapter 3

Results and Discussion

3.1 Effect of rib spacing

By extracting the plots for textiles with the same surface coating and rib height, one can compare these and see the effect of varying the rib spacing. This is done for the C_D-Re curves in figures 3.1a, 3.3a, 3.4a and 3.5a, and, for the corresponding St-numbers in figures 3.1b, 3.3b, 3.4b and 3.5b. The results for the smooth cylinder are also plotted as a benchmark.

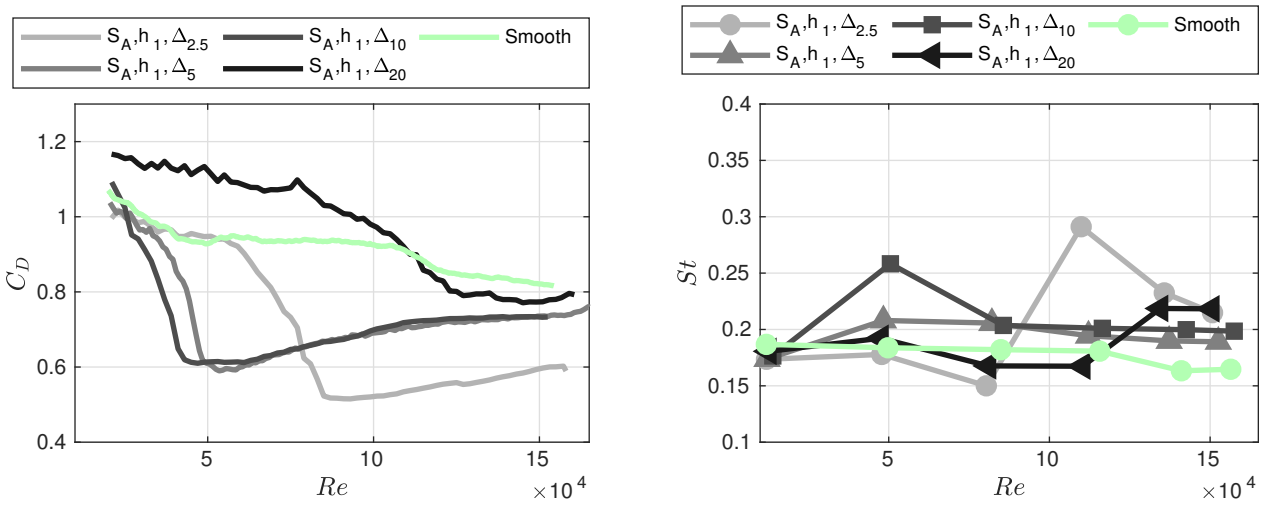

(a) C_D-Re (b) St-Re

Figure 3.1: Effect on C_D-Re curve by varying the rib spacing, for coating fabric A and $h/d = 0.0133$.

Figure 3.1a shows that for coating fabric A and relative rib height $h/d = 0.0133$, relative rib spacing $\Delta/h = 10$ ($S_C A, h_1, \Delta_{10}$) gave the lowest Re_c, $\Delta/h = 2.5$ ($S_A, h_1, \Delta_{2.5}$) gave the lowest $C_{D,m}$ and $\Delta/h = 20$ (S_A, h_1, Δ_{20}) gave both the largest Re_c and $C_{D,m}$ of the four. There is thus a trend where increasing rib spacing increases $C_{D,m}$, and decreases Re_c until a point where the Re_c starts to increase again. This would indicate that there is one rib spacing that would give the smallest Re_c. This trend is also indicated in figure 3.2a. This might seem counter-intuitive as one would expect that adding more ribs (decreasing rib spacing) would increase the roughness, hence reducing Re_c. An explanation of this might be that for very large rib spacings, the spacing is so large that the incoming flow angle plays a large roll in the drag reduction. In general, savings

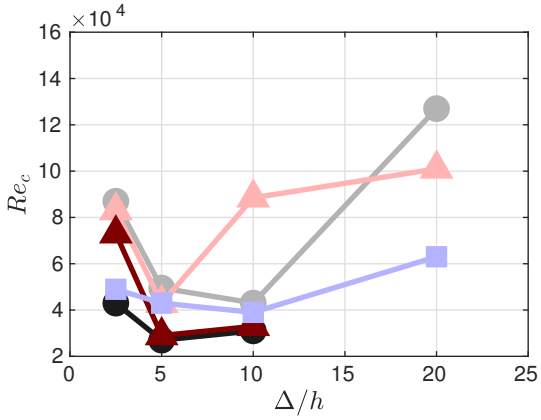

(a) Critical Reynolds number vs relative rib spacing for different relative rib heights and coating fabrics.

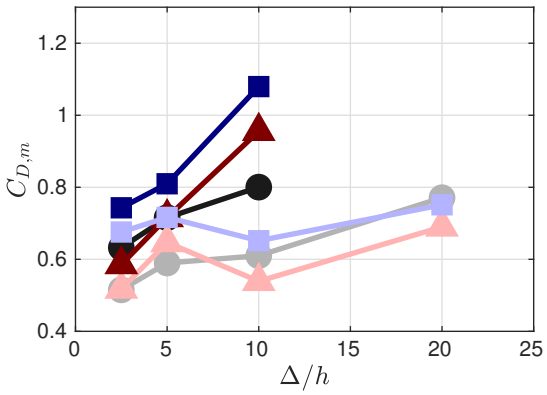

(b) Minimum drag coefficient vs relative rib spacing for different relative rib heights and coating fabrics.

Figure 3.2: The effect on Re_c and $C_{D,m}$ by varying the relative rib spacing is plotted. The different curves have different coating and relative rib height. Square points are for coating C, circles for A and triangles for B. Darker colour means larger rib height.

that are dependent on the incoming flow angle are undesirable as in many applications (e.g., buildings, sports aerodynamics) the incoming flow angle is not controllable. For very small rib spacings, the flow will perceive the individual ribs to a lesser and lesser degree, effectively only increasing the surface area and skin friction. Another explanation might also be that the surface coating has caused some smoothing effect of the ribbed surface geometry, for the smallest rib spacings, and as shown in the figures and previous studies, the drag crisis of a smooth cylinder happens later than many of the coated cylinders investigated here.

The dependence of St on Re is plotted for the same cases in figure 3.1b. In these curves, there are peaks at, or near, Re_c for the $\Delta/h = 2.5$, 10 and 20 cases. For $\Delta/h = 5$ (S_A, h_1, Δ_5), a peak at the critical Reynolds number is not visible. This is likely because the second Re tested is slightly lower than Re_c for this case, and thus the peak may have been missed. The general trend seems to be that St is constant or slightly decreasing in the subcritical and critical flow regime until Re_c is reached. At Re_c, St rapidly increases and then decreases through the supercritical flow regime. The smooth cylinder measured in this case is subcritical throughout the entire tested Re range, but the trends are consistent with the results obtained by Schewe [3] for the smooth cylinder around Re_c. The St at both the peaks and in the subcritical regime varies for the different cases. This means that varying the rib spacing changes the shedding frequency. There also appears to be a relation between the St peak and C_D itself, as the surface with the lowest $C_{D,m}$ gives the largest St peak. For surface coating A and relative rib height $h/d = 0.0267$, the trends are similar.

Changing the surface coating to type B and the relative rib height to 0.0133 gave figures 3.3a and 3.3b. These C_D-Re curves do not show the exact same trend as seen for coating A. For coating B, $\Delta/h = 5$ (S_B, h_1, Δ_5) produces the lowest Re_c, while $\Delta/h = 10$ (S_B, h_1, Δ_{10}) and $\Delta/h = 2.5$ ($S_B, h_1, \Delta_{2.5}$) yields more or less the same curve. Moreover, for $120,000 < Re < 160,000$, the curves for $\Delta/h = 5$ and 20 (S_B, h_1, Δ_5 and S_B, h_1, Δ_{20}) collapse into one curve and in fact all four curves are quite similar. This suggests that while the ribs may change Re_c, this surface coating may dominate the supercritical drag for ribs of this height.

Increasing the relative rib height to 0.0267 for coating B, and varying the rib spacing gives the same trend as mentioned earlier for surface coating A. The $C_{D,m}$ varies extensively for the three cases and increases for increasing spacing, yielding approximately 0.6, 0.7 and 0.95 for S_B, h_2, Δ_5, S_B, h_2, Δ_{10} and S_B, h_2, Δ_{20}, respectively.

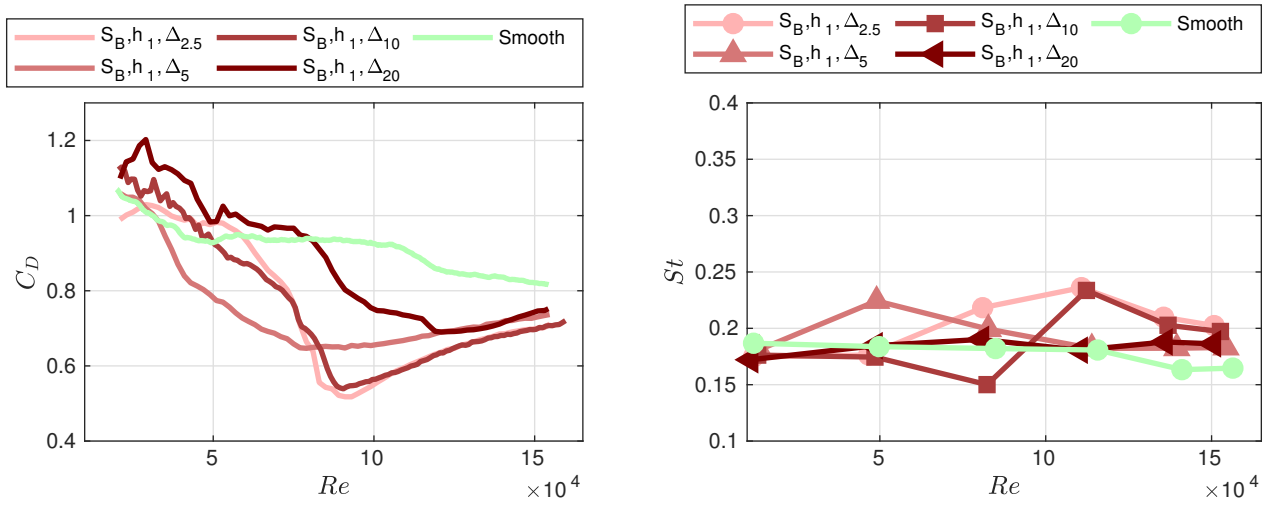

(a) C_D-Re (b) St-Re

Figure 3.3: Effect on C_D-Re curve and St by varying the rib spacing Δ, for coating fabric B and relative rib height 0.0133.

The St-numbers in figure 3.4b seem to create peaks at Re_c, but these peaks are very small (barely above 0.2) compared to the ones seen for $h/d = 0.0133$ and the one for the smooth cylinder (approximately 0.4) shown by Schewe [3]. For $\Delta/h = 10$ (S_B, h_2, Δ_{20}) though, the St seem to be relatively constant with Re. This could indicate that the St-peak vanishes for large rib spacings and increasing rib height.

Plotting results for surface coating C, relative rib height 0.0133 and different rib spacings give figures 3.5a and 3.5b. The Re_c appear to roughly follow the same trend as mentioned earlier, with decreasing Re_c from $\Delta/h = 2.5$ ($S_C, h_1, \Delta_{2.5}$) through $\Delta/h = 5$ (S_C, h_1, Δ_5) up to $\Delta/h = 10$ (S_C, h_1, Δ_{10}), before increasing again for $\Delta/h = 20$ (S_C, h_1, Δ_{20}). The variation between cases for the three smallest spacings are small compared to the changes for the other coatings (max. Re_c difference of 15,000), compared to a Re_c increase between S_C, h_1, Δ_{10} and S_C, h_1, Δ_{20} of approximately 50,000. $C_{D,m}$ is in this case smallest for S_C, h_1, Δ_{10} and largest for S_C, h_1, Δ_{20}, but the variations are small for this surface coating which is the roughest coating of the three. One can also notice that the curves for $S_C, h_1, \Delta_{2.5}$ and S_C, h_1, Δ_{10} collapse in the supercritical and transcritial ranges, and the variations in C_D for the four curves are relatively small (approximately 0.05) for $80,000 < Re < 150,000$. This suggests again that the rougher surface coatings dominate the supercritical regime, playing a more significant roll there than the ribs.

From figure 3.5b one can see that St curves for the three smallest rib spacings are approximately collapsed; they also have similar C_D-Re curves and hence Re_c. Such a correlation would again indicate that the St is, in addition to its peak being correlated to Re_c, correlated to C_D itself.

Increasing the relative rib height to 0.0267 for coating C, yields the same trends as mentioned earlier. Re_c decreases and $C_{D,m}$ increases for an increase in the rib spacing from $\Delta/h = 2.5$ (S_C, h_2, Δ_5) to $\Delta/h = 5$ (S_C, h_2, Δ_5). Both Re_c and $C_{D,m}$ then increases for an increase in rib spacing up to $\Delta/h = 10$ (S_C, h_2, Δ_{20}).

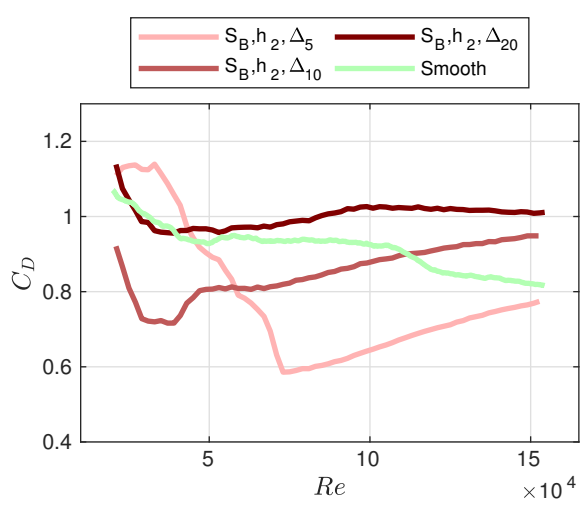

(a) C_D-Re

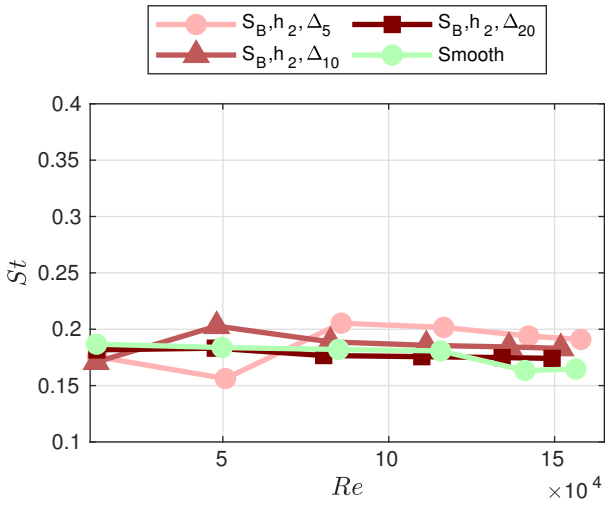

(b) $St - Re$

Figure 3.4: Effect on C_D-Re curve and St by varying the rib spacing, for coating fabric B and relative rib height 0.0267.

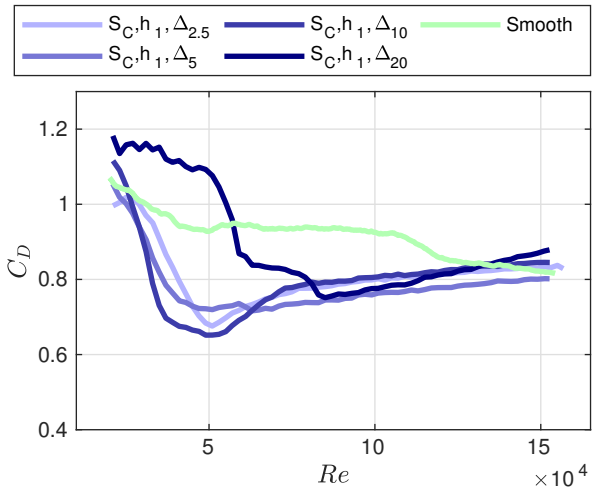

(a) C_D-Re

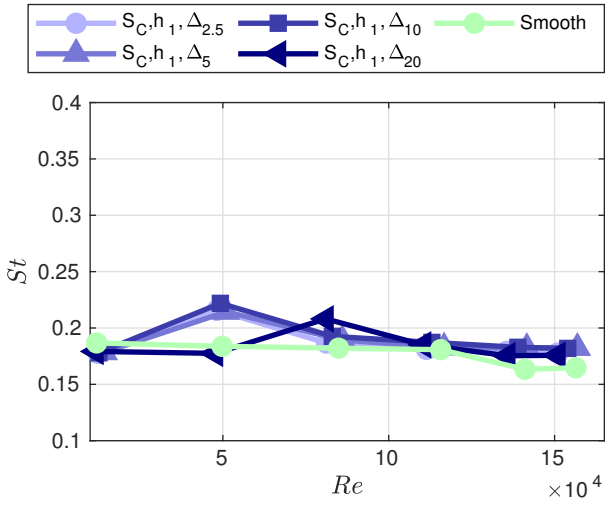

(b) St-Re

Figure 3.5: Effect on C_D-Re curve and St by varying the rib spacing, for coating fabric C and relative rib height 0.0133.

To summarise, there appears to be a rib spacing that optimises Re_c to a minimum value for the cylinder for all tested cases. This is indicated in figure 3.2a. Increasing the rib spacing too much, might cause the effects on the flow to be more dependent on the actual positions of the ribs than the spacing between them. This appears to be the effect for all the tested cases with a rib spacing of 20 mm ($\Delta/d = 0.267$). This rib spacing, for this cylinder diameter, seem to be of no interest from an engineering standpoint. In nearly all applications, passive control drags savings that are dependent on the incoming flow direction are far from ideal. Different orientations are not investigated here, but symmetric rib positions were maintained for all tests and geometries. Smaller spacings than the ”optimal”, seem to cause a smoothing effect on the surface as the grooves between the ribs becomes narrow. This effect might also be caused by the coating fabric, which smoothens the edges around the root of the ribs. This effect might become larger with smaller rib spacings, causing a rounder groove than for larger spacings. In terms of the minimum drag, the spacing appears to generally increase the minimum drag. Thus, based on rib spacing alone, $\Delta/h = 5$ appears to optimise Re_c and generally it appears desirable to keep the spacing small to maintain a low $C_{D,m}$.

3.2 Effect of rib height

The effect of rib height is addressed in this section by comparing cases where this is the only parameter varied. By keeping surface coating A and the relative spacing at 2.5, one can produce figure 3.6. No ribs and coating A (S_A, h_0) and also the smooth cylinder are plotted to imitate a rib height of 0. The smooth cylinder and S_A, h_0 are still subcritical in the measured Re domain, as seen in figure 3.6a, and thus those cases provide no information about its Re_c or $C_{D,m}$ other than that the drag crisis occurs at a higher Re. This reduces the information down to two points, giving an increase in $C_{D,m}$ and a decrease in Re_c when increasing the relative rib height from 0.0133 ($S_A, h_1, \Delta_{2.5}$) to 0.0267 (S_A, h_2, Δ_5).

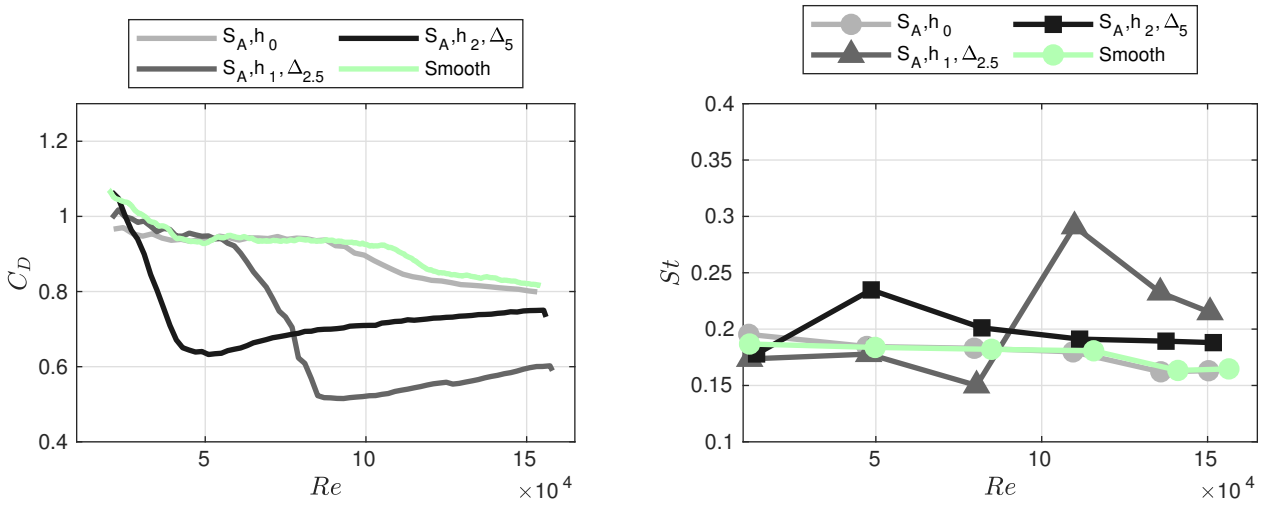

(a) C_D-Re (b) St-Re

Figure 3.6: Effect on the C_D-Re curve and the St by varying the rib height, for coating fabric A and relative rib spacing $\Delta/h = 2.5$.

From figure 3.6b, St can be compared for the three cases. Whilst S_A, h_0 has subcritical St values, $S_A, h_1, \Delta_{2.5}$ and S_A, h_2, Δ_5 give peaks at their respective Re_c. These peaks are different

and larger for the smallest rib height. This might indicate a tendency of decreasing St peak for increasing rib height.

Increasing the relative rib spacing to 5, keeping surface coating A and varying the rib height shows the same trend of increasing $C_{D,m}$ and decreasing Re_c when increasing the relative rib height from 0.0133 (S_A, h_1, Δ_5) to 0.0267 (S_A, h_2, Δ_{10}).

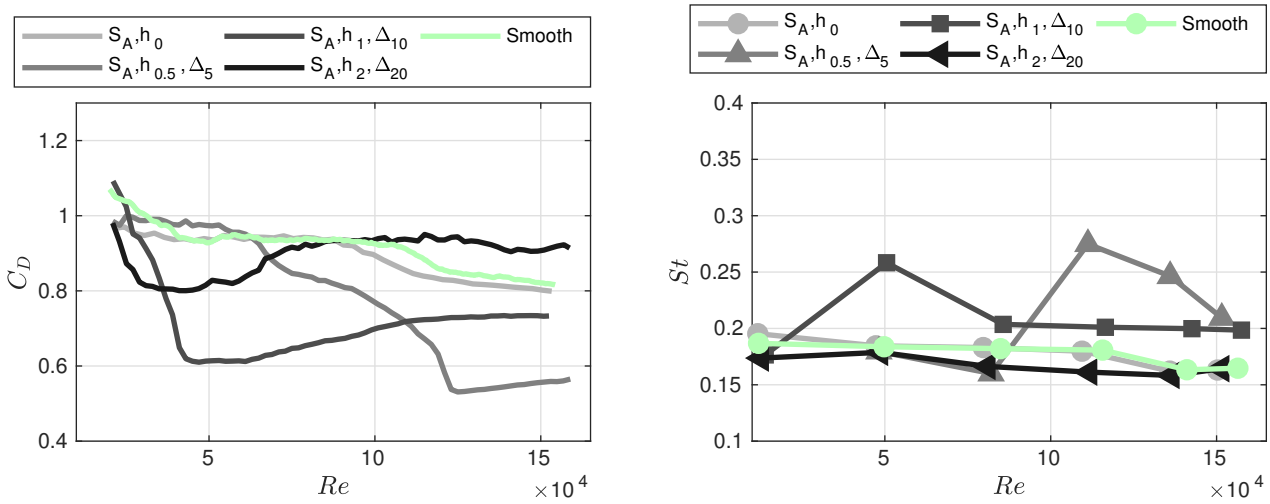

(a) C_D-Re (b) St-Re

Figure 3.7: Effect on C_D-Re curve and St by varying the relative rib height, for coating fabric A and relative rib spacing 10.

Figure 3.7 show results for coating A and relative spacing 10. The C_D-Re curves in figure 3.7a show a non-linear correlation with decreasing Re_c and increasing $C_{D,m}$ for increasing the relative rib height from 0.0067 ($S_A, h_{0.5}, \Delta_5$) through 0.0133 (S_A, h_1, Δ_{10}) to 0.0267 (S_A, h_2, Δ_{20}).

Looking at St, the same trends as mentioned earlier, with a decreasing peak for increasing relative rib height, can be seen. For S_A, h_2, Δ_{20}, if the second measurement can be seen to correspond to Re_c, the peak vanishes completely.

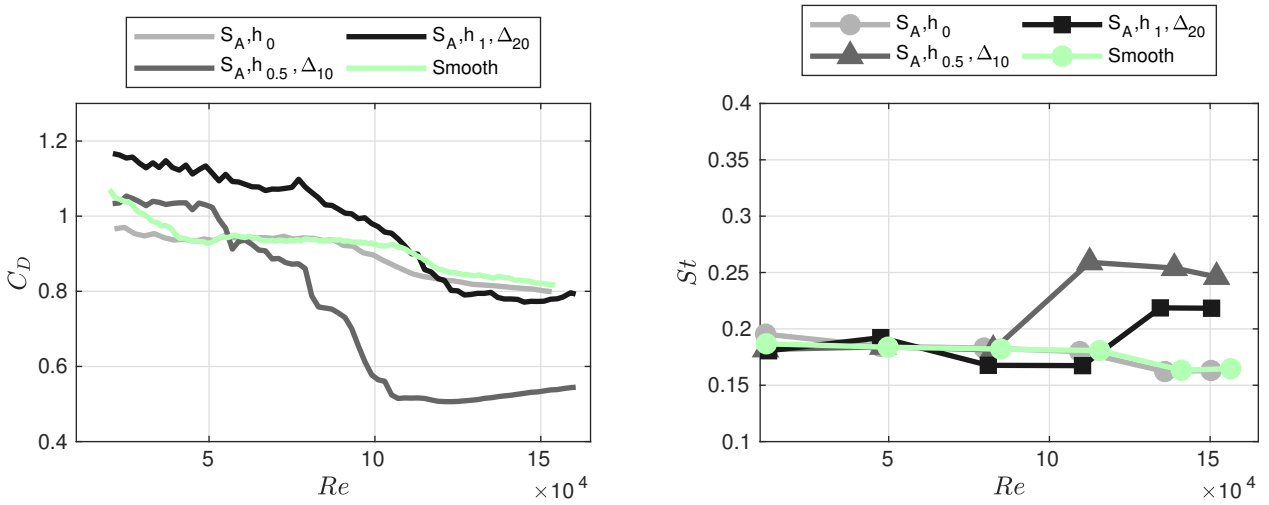

(a) C_D-Re (b) St-Re

Figure 3.8: Effect on C_D-Re curve and St by varying the relative rib height, for coating fabric A and relative rib spacing 20.

For relative spacing 20 and coating fabric A, results are shown in figure 3.8. Comparing the C_D-Re curves in figure 3.8a shows that increasing the relative rib height from 0 (S_A, h_0) to 0.0067 ($S_A, h_{0.5}, \Delta_{10}$) and further up to 0.0133 (S_A, h_1, Δ_{20}), increases the subcritical C_D and $C_{D,m}$. Re_c is decreasing going from S_A, h_0 to $S_A, h_{0.5}, \Delta_{10}$, but increasing from $S_A, h_{0.5}, \Delta_{10}$ to S_A, h_1, Δ_{20}. This is probably due to, as previously discussed, the large spacing for S_A, h_1, Δ_{20} causing non-efficient rib positions.

The effects on the corresponding St are shown in figure 3.8b. The peak at Re_c deteriorates when increasing the relative rib height from $S_A, h_{0.5}, \Delta_{10}$ to S_A, h_1, Δ_{20}. However, the peaks themselves for these two cases are stable when increasing Re. This might be due to the very flat supercritical slope in the C_D-Re. This is also the case for $S_A, h_{0.5}, \Delta_5$ as seen in the previously discussed case in figure 3.7a. That might indicate a correlation between the St-number and the slope of the C_D-Re curve in the supercritical range, where a steep slope suppresses the St-peak. This corresponds to what was found by Schewe [3], who showed that the St peak suddenly vanished when increasing Re into the supercritical range.

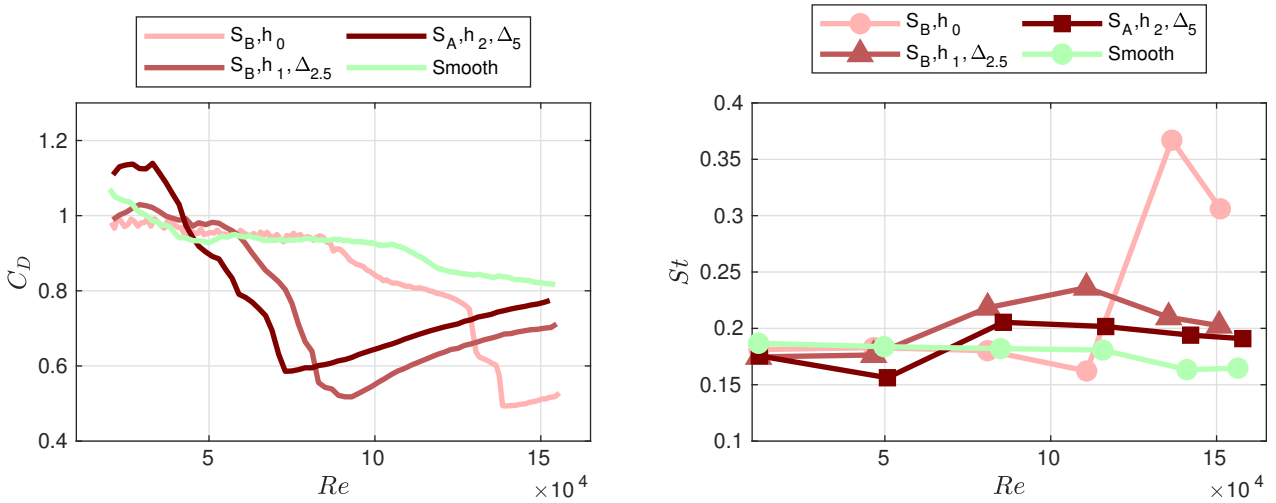

(a) C_D-Re (b) St-Re

Figure 3.9: Effect on C_D-Re curve and St by varying the rib height, for coating fabric B and relative rib spacing 2.5.

The analysis of the previous cases for the four different relative spacings can be repeated using coating fabric B instead of A. The results for coating fabric B and relative spacings 2.5, 5, 10 and 20 show the same trends with minor differences. The general trend in these four cases is very clear, and can be seen in figures 3.9 for relative spacing 2.5. Increasing the relative rib height results in a decreasing Re_c, an increasing subcritical C_D, an increasing $C_{D,m}$ and a decreasing St peak value. The supercritical C_D-Re slope doesn't seem to be generally affected by the relative rib height, which indicates that the slope is affected by either the rib spacing and/or the micro-roughness instead. These trends can explain the effect on all parameters for all the textiles with coating fabric B except one parameter; Re_c for S_B, h_1, Δ_{20}, which is larger than for the smaller rib height $S_B, h_{0.5}, \Delta_{10}$. This might be due to S_B, h_1, Δ_{20} having, as previously discussed, a high dependence on the incoming flow angle, which would make it undesirable as a passive drag reduction method anyway.

Repeating the analysis for the four relative spacings, but with coating fabric C, results in many of the same trends as seen for coating fabric B with a few exceptions. Firstly, figure 3.10 shows results for relative spacing 2.5. From the C_D-Re curves in figure 3.10a one can see that increasing the rib height result in a decreasing Re_c, an increasing $C_{D,m}$ and a flatter supercritical slope. So,

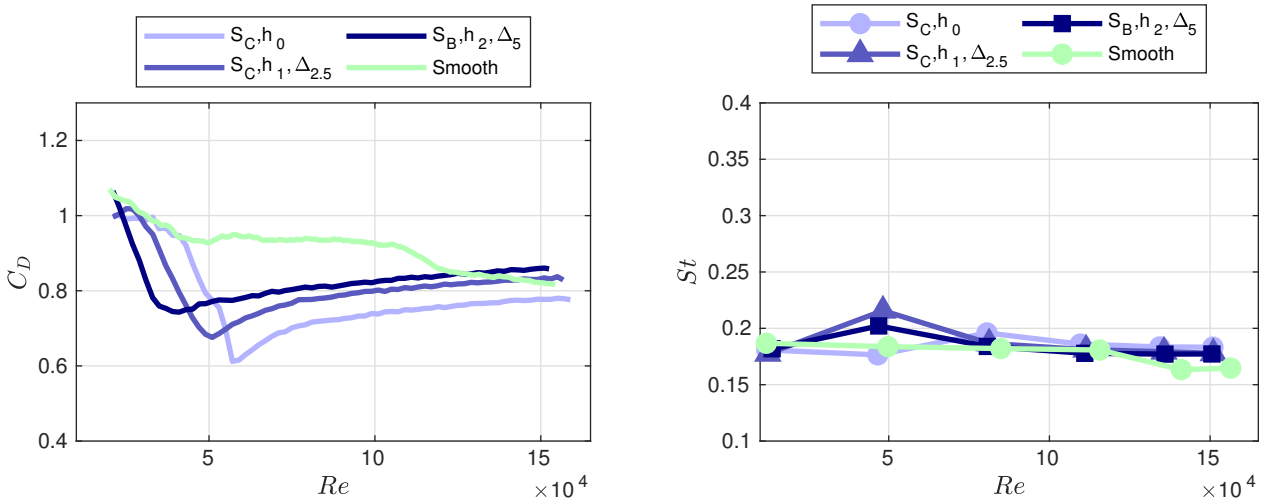

(a) C_D-Re (b) St-Re

Figure 3.10: Effect on C_D-Re curve and St by varying the relative rib height, for coating fabric C and relative rib spacing 2.5.

while the supercritical slopes for coating fabric B are unaffected by the relative rib height, the slopes for the same rib geometries are effected by the relative rib height when covered by coating fabric C.

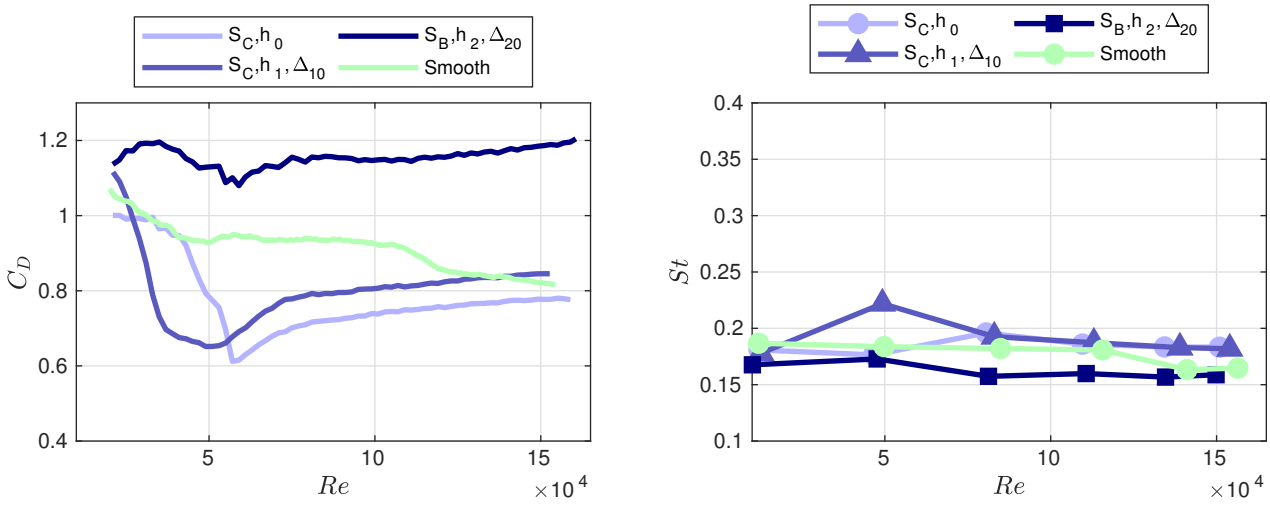

(a) C_D-Re (b) St-Re

Figure 3.11: Effect on C_D-Re curve and St by varying the relative rib height, for coating fabric C and relative rib spacing 10.

Relative spacing 5 shows the same trends, but for relative spacing 10, in figure 3.12a, the slopes are again very similar. Besides the varying trend in the supercritical slopes for coating C and relative spacings 2.5, 5 and 10, there is still the similarities of decreasing Re_c, increasing $C_{D,m}$, increasing subcritical C_D and increasing transcritical C_D, for increasing rib height. All curves except S_C, h_2, Δ_{20} follow this trend. It is difficult to comment on St in these cases, as the St peak for no ribs (S_C, h_0) is not visible. Nonetheless, as the magnitude of the St peak decreases for the rest of the textiles for increasing rib height, one should expect that C0 has the St peak of largest magnitude. This would mean a trend of decreasing St for increasing rib height, as also previously

shown.

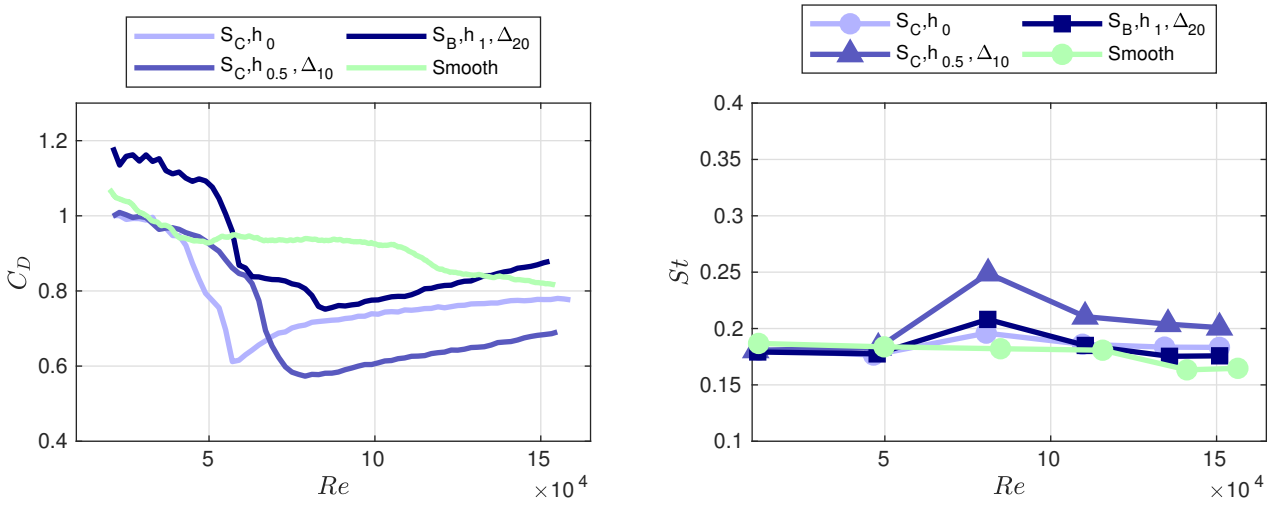

(a) C_D-Re (b) St-Re

Figure 3.12: Effect on C_D-Re curve and St by varying the relative rib height, for coating fabric C and relative rib spacing 20.

The results for relative spacing 20 and coating C in figure 3.12 doesn't show these same trends. Here, going from no ribs (S_C, h_0) to $h/d = 0.0067$ ($S_C, h_{0.5}, \Delta_{10}$), $C_{D,m}$ decreases, Re_c increases and the supercritical slope flattens. This would indicate that adding certain ribs to a surface of this micro-roughness basically makes a smoother surface. The supercritical range is, however, prolonged and the transcritical range has not been reached at the end of the measured Re domain.

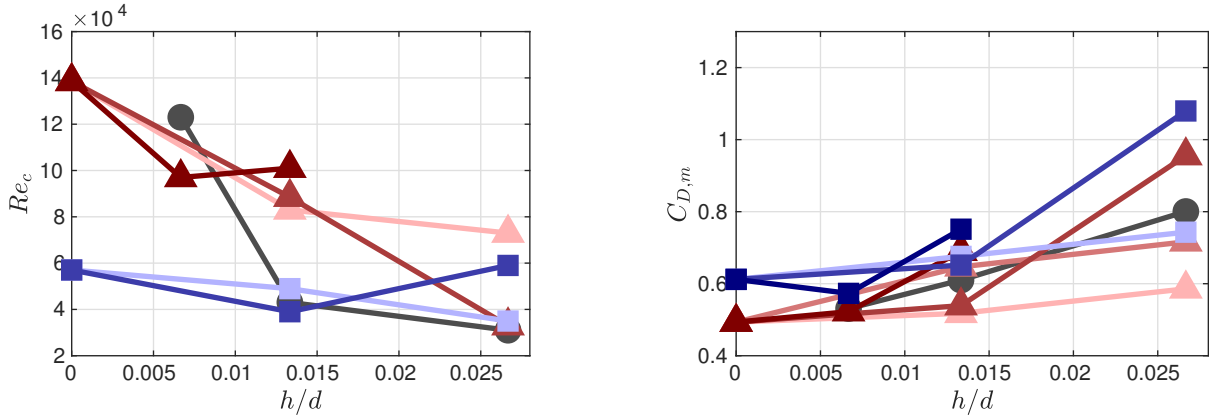

(a) Critical Reynolds number vs relative rib height. (b) Minimum drag coefficient vs relative rib height.

Figure 3.13: The effect on Re_c and $C_{D,m}$ by varying h/d is plotted. The different curves have different coating and relative rib spacing. Square points are for coating C, triangles for B and circles for A. Darker colour means larger rib height.

Summarising the general trend found in this section, increasing the relative rib height for a given relative spacing and coating fabric results in a decrease of Re_c, and $C_{D,m}$, $C_{D,s}$ and $C_{D,t}$ increase. These trends are clearly illustrated in figure 3.13, which sums up the effect on $C_{D,m}$ and Re_c. Also, the critical and supercritical slope seem to be unaffected by varying the rib height. This is the general trend for the C_D-Re curve, except in the case where ribs with $h/d = 0.0067$

are added to a cylinder with a rough surface. Then, the result is a textile that behaves like a smoother surface. The general trend for St is a decreasing amplitude for the St peak near the Re_c.

3.3 Effect of surface coating

It is also interesting to see what effect the micro-roughness has on the results. This effect can be shown by extracting plots for textiles of equal relative rib height and relative spacing, but different coating fabrics.

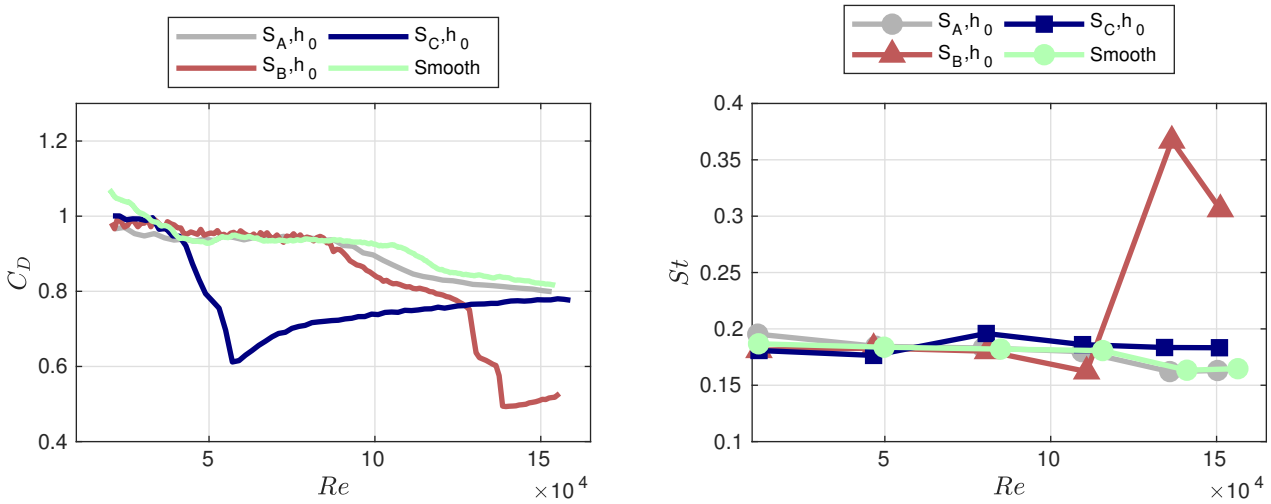

(a) C_D-Re (b) St-Re

Figure 3.14: Effect of varying the coating fabric for textiles without ribs.

To get an initial impression of the general effect of changing the micro-roughness, one can look at figure 3.14. Here, three cases are shown for textiles without ribs and varying coating fabrics, alongside the smooth cylinder. Figure 3.14a shows that for the smoothest coating fabric (S_A, h_0), the curve is still subcritical or approaching the critical range at the end of the measured Re-domain. As the micro roughness is increased to coating fabric B (S_B, h_0), the Re_c is reduced to approximately 140,000. Again, increasing the micro-roughness to coating fabric C (S_C, h_0) decreases the Re_c to approximately 60,000 while increasing the $C_{D,m}$ from roughly 0.5 to 0.6. This means that an increase in micro-roughness shifts the point of the $C_{D,m}$ to larger C_D and lower Re. This corresponds to what would be expected by the relative roughness model. The St-numbers in figure 3.14b show one large peak of approximately 0.37 for S_B, h_0 at Re_c. This peak can not be seen for S_C, h_0, but the measured points closest to Re_c are at the start of the critical range and at the end of the supercritical range. The amplitude of the peak can therefore not be seen and compared to S_B, h_0.

Changing the relative rib height to 0.0067 and the relative rib spacing to 20 yields the results as shown in figure 3.15. One can see from figure 3.15a that the trajectory of the C_D-Re curves for coating fabric A ($S_A, h_{0.5}, \Delta_{10}$) and B ($S_B, h_{0.5}, \Delta_{10}$) are very similar besides a slightly lower Re_c for $S_B, h_{0.5}, \Delta_{10}$. Increasing the micro-roughness further to coating fabric C ($S_C, h_{0.5}, \Delta_{10}$), decreases Re_c and increases $C_{D,m}$. St in figure 3.15b shows distinct peaks at the corresponding Re_c followed by a slow decrease for increasing Re. The peak is largest for $S_B, h_{0.5}, \Delta_{10}$ at approximately 0.3 and approximately the same for $S_A, h_{0.5}, \Delta_{10}$ and $S_C, h_{0.5}, \Delta_{10}$, at around 0.25. The decrease after the peak is slower for $S_A, h_{0.5}, \Delta_{10}$ than for $S_C, h_{0.5}, \Delta_{10}$.

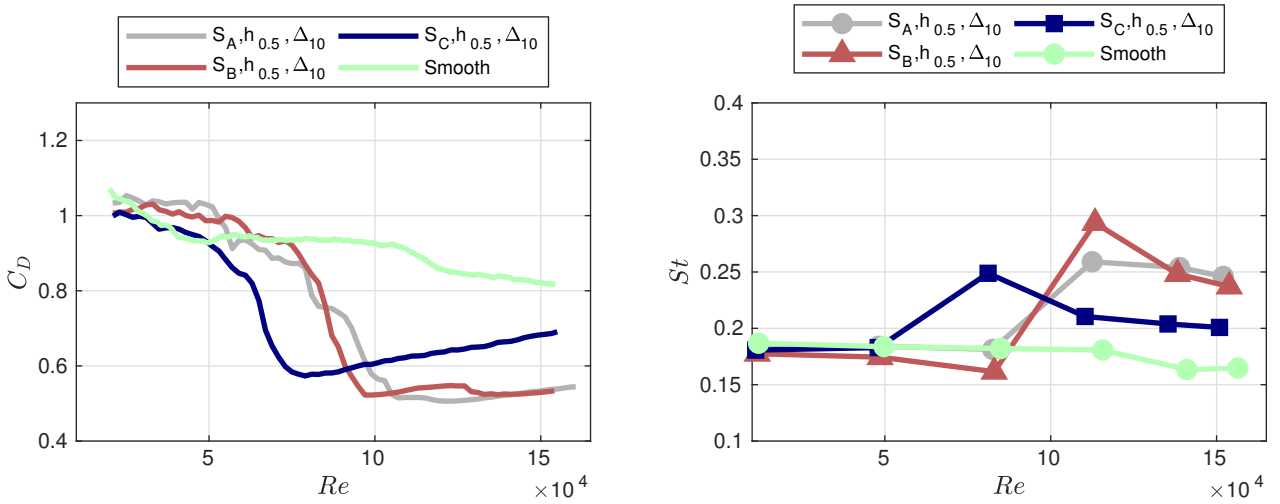

(a) C_D-Re (b) St-Re

Figure 3.15: Effect of varying the coating fabric for textiles with $h/d = 0.067$ and $\Delta/h = 20$.

Figure 3.16 shows results for the textiles with relative rib height 0.0133 and relative rib spacing 2.5. As was also the case for the previous case, figure 3.16a shows that the C_D-Re curves for coating fabric A ($S_A, h_1, \Delta_{2.5}$) and B ($S_B, h_1, \Delta_{2.5}$) are very similar in the subcritical and critical flow range. In the supercritical range though, the curves diverge with a steeper supercritical slope for $S_B, h_1, \Delta_{2.5}$ than for $S_A, h_1, \Delta_{2.5}$. The slope for $S_B, h_1, \Delta_{2.5}$ is also more curved than for $S_A, h_1, \Delta_{2.5}$ which has an almost linear supercritical range. Re_c for coating C ($S_C, h_1, \Delta_{2.5}$) is almost halved from the other textiles and $C_{D,m}$ increased by approximately 0.2. St in figure 3.16b shows a decreasing St peak by increasing the micro-roughness from coating A to C. This might indicate that there are some roughness peaks in the coating fabrics that inhibit the vortex shedding at Re_c. However, the previous case did not show this trend.

The textiles with relative rib height 0.0133 and relative spacing 5 follows similar trends to the previous, but has an extended transitional range.

For relative rib height 0.0133 and relative spacing 10 in figure 3.17 though, the trend is different. Here, coating B (S_B, h_1, Δ_{10}) gives the lowest $C_{D,m}$ and largest Re_c, and emerges as the smoother textile. This is counter-intuitive to what has been indicated in the previous cases, where coating fabric A clearly indicates having a smoother micro-roughness than coating fabric B. However, looking away from this incongruity in the overall trend and further on to the supercritical slope, the slope seem to be steeper for S_B, h_1, Δ_{10} than for S_A, h_1, Δ_{10} and actually move past S_A, h_1, Δ_{10} to give larger $C_{D,t}$ for Re above the tested domain. Coating C (Cr1d10) gave an even steeper supercritical slope than S_B, h_1, Δ_{10}, giving basis for modelling the supercritical slope, and maybe $C_{D,t}$, as a function of the micro-roughness.

Figure 3.18 gives results for relative rib height 0.0133 and relative rib spacing 20. Also here, the Cd-Re curves in figure 3.18a show a trend for $C_{D,m}$ which is incongruous with the overall trend, as $C_{D,m}$ for coating A (S_A, h_1, Δ_{20}) is slightly larger than for both B (S_B, h_1, Δ_{20}) and C (S_C, h_1, Δ_{20}). The Re_c are as expected with a decreasing value for increasing micro-roughness, going from A (S_A, h_1, Δ_{20}) through S_B, h_1, Δ_{20}, to S_C, h_1, Δ_{20}. Another tendency for this case might seem to be an increasing steepness of the critical slope with increasing micro-roughness.

As the St peaks themselves are of low values compared to previously discussed cases, it is hard to see any other trends in the effect on the vortex shedding than already discussed.

The results for relative rib height 0.0267 and relative rib spacing 2.5 show the same tendency as previously shown for relative rib height 0.0133 and relative rib spacing 10 in figure 3.17.

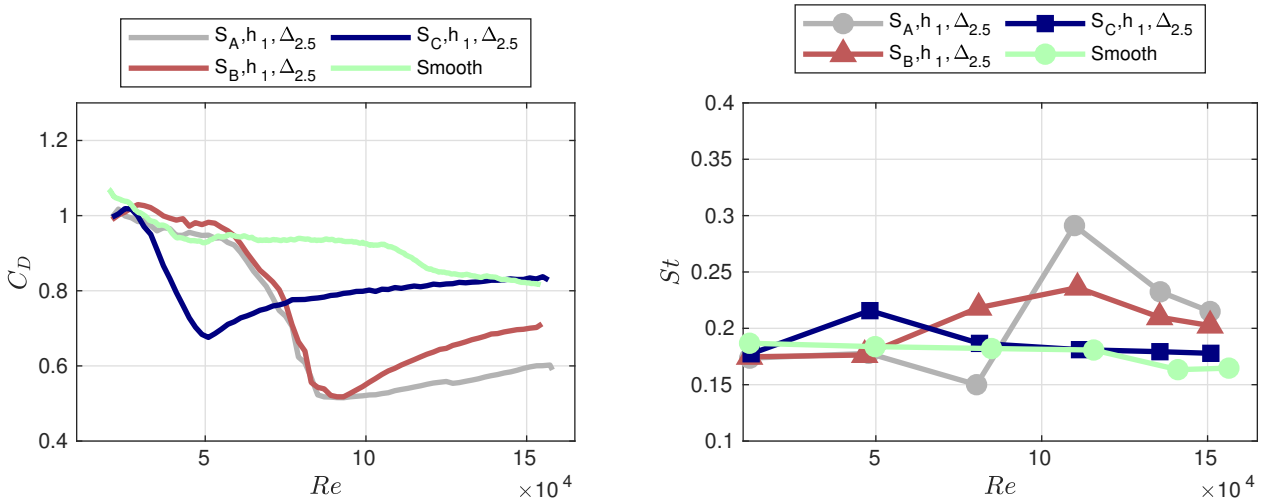

(a) C_D-Re (b) St-Re

Figure 3.16: Results for textiles with relative rib height 0.0133 and relative rib spacing 2.5.

The results for relative rib height 0.0267 and relative rib spacing 5 in figure 3.19 again show C_D-Re curves for coating A (S_A, h_2, Δ_5) and B (S_B, h_2, Δ_{10}) which follows approximately the same trajectory all the way until the transcritical regime for S_A, h_2, Δ_{10}. Here, S_B, h_2, Δ_{10} continues to increase while S_A, h_2, Δ_{10} reaches a constant $C_{D,t}$. Unless S_B, h_2, Δ_{10} would cross above the curve for coating C (S_C, h_2, Δ_{10}) for higher Re than the measured domain, the previously shown trend of increasing $C_{D,t}$ for increasing micro-roughness stands.

As the relative rib spacing is increased to 10 in figure 3.20, one can again see that the positive effect of the ribs more or less disappear for this rib spacing. The C_D-Re curves for coating A (S_A, h_2, Δ_{20}), B (S_B, h_2, Δ_{20}) and C (S_C, h_2, Δ_{20}) doesn't intersect and yields larger C_D for increasing micro-roughness throughout the Re domain, and even with $C_{D,t}$ for S_B, h_2, Δ_{20} and S_C, h_2, Δ_{20} that overcomes $C_{D,s}$ for S_B, h_0 and S_C, h_0, respectively.

To summarise, increasing the surface's micro-roughness generally decreases Re_c, increases $C_{D,m}$, increases $C_{D,t}$ and increases the steepness of the supercritical slope. This is indicated in figure 3.21.

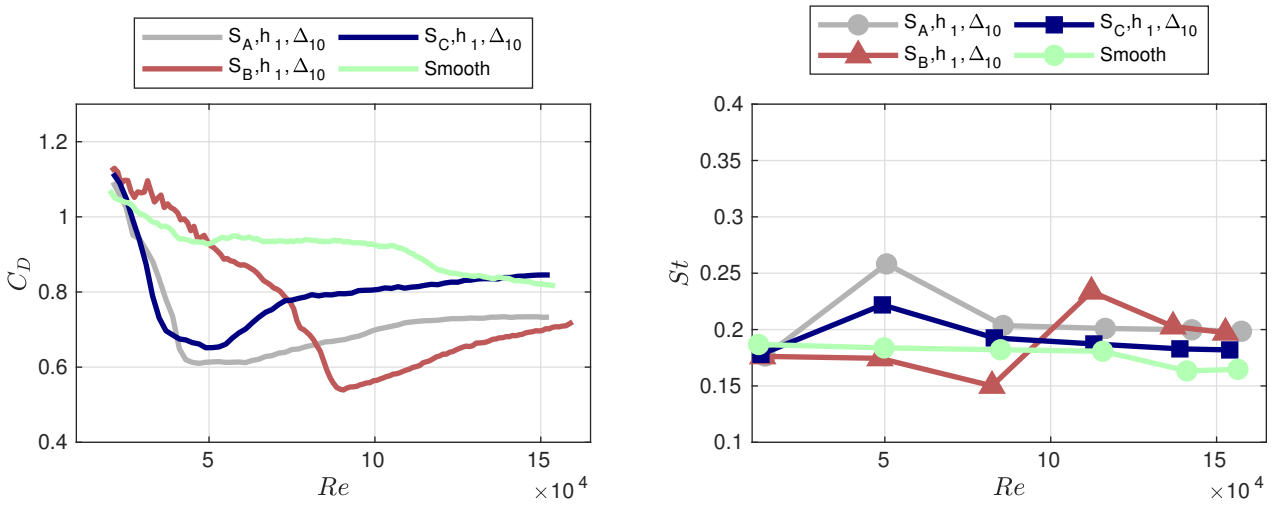

(a) C_D-Re (b) St-Re

Figure 3.17: Effect of varying the coating fabric for textiles with $h/d = 0.133$ and $\Delta/h = 10$.

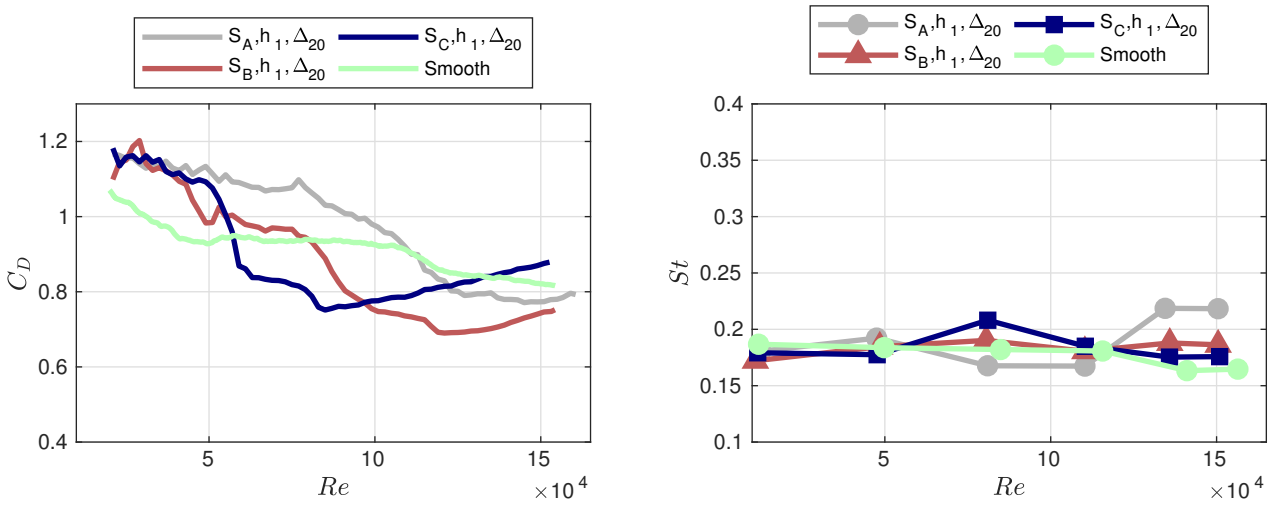

(a) C_D-Re (b) St-Re

Figure 3.18: Effect of varying the coating fabric for textiles with $h/d = 0.133$ and $\Delta/h = 20$.

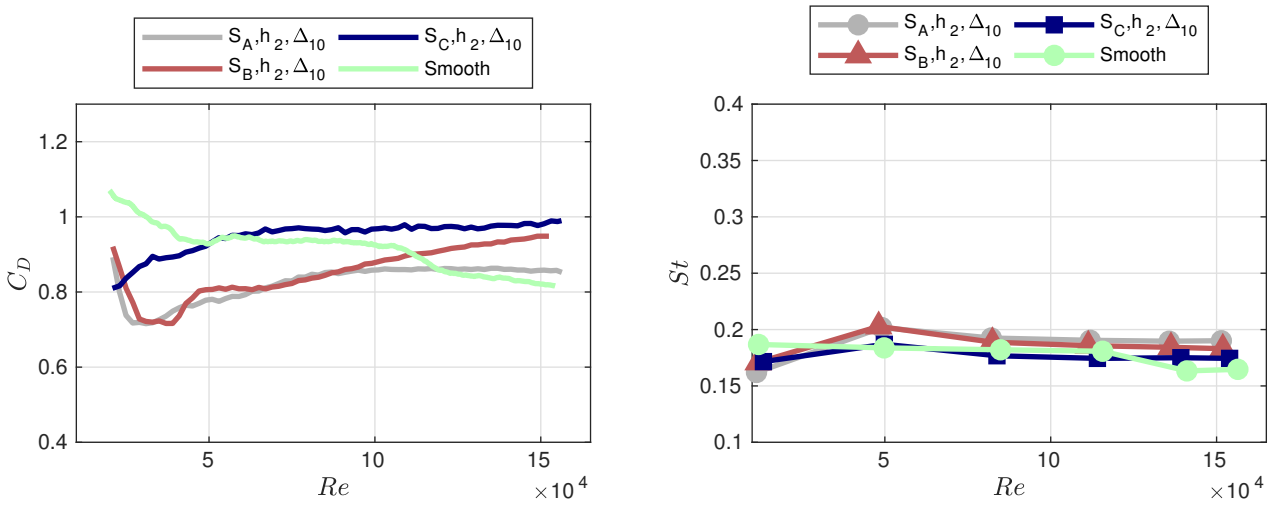

(a) C_D-Re (b) St-Re

Figure 3.19: Effect of varying the coating fabric for textiles with $h/d = 0.0267$ and $\Delta/h = 5$.

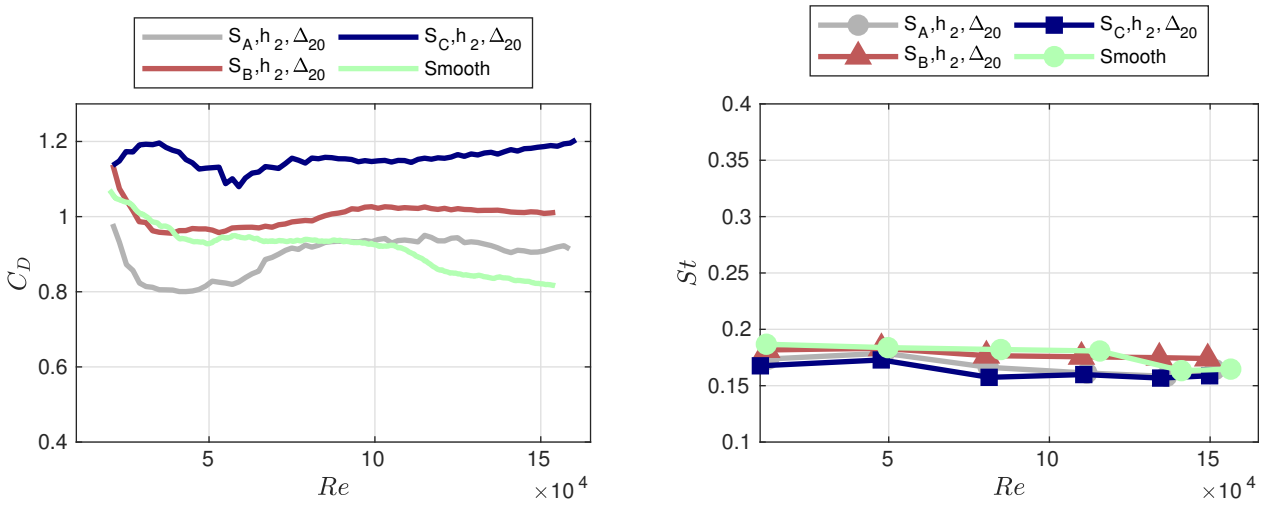

(a) C_D-Re (b) St-Re

Figure 3.20: Effect of varying the coating fabric for textiles with $h/d = 0.0267$ and $\Delta/h = 10$.

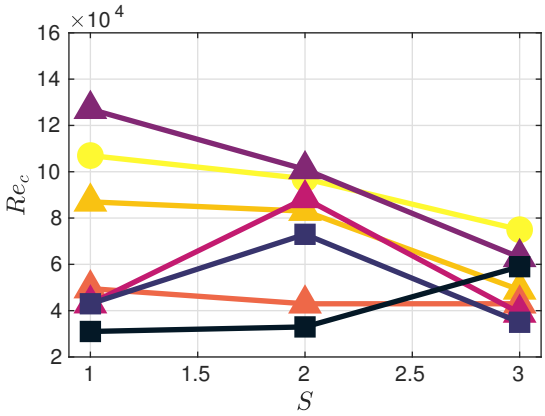

(a) Critical Reynolds number vs coating fabric.

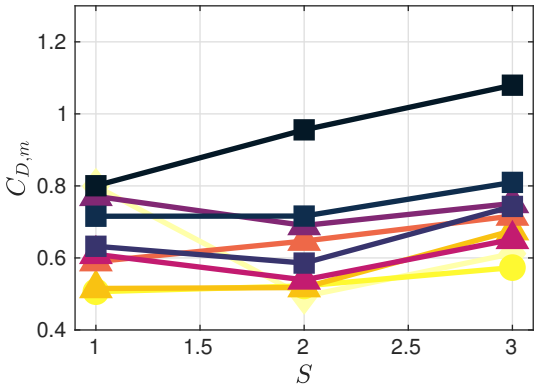

(b) Minimum drag coefficient vs coating fabric.

Figure 3.21: The effect on Re_c and $C_{D,m}$ by varying the surface coating is plotted. $S = 1$ means coating A, $S = 2$ means coating B and $S = 3$ means coating C. The different curves have different relative rib height and rib spacing. Lines with circles have $h/d = 0.0067$, triangles have $h/d = 0.0133$ and squares have $h/d = 0.0267$. Darker colour means larger rib spacing.

Chapter 4

Global results

4.1 Average drag coefficient

From an engineering standpoint, it is interesting to know which of the surface structures is the best for a cylinder in any given situation. This would be dependent on the Re range the cylinder will experience, and in most cases the cylinder will experience a flow where the Re lies within a certain domain. It is therefore interesting to analyse the average C_D, $C_{D,\text{avg}}$, across different Re ranges rather than just a singular C_D at one Re.

In figure 4.1, $C_{D,\text{avg}}$ for all textiles, across the entire measured Re range, has been plotted. One can see that $C_{D,\text{avg}}$ across the measured Re range varies all the way from 0.7 to 1.16 for the textiles tested. The textiles with the largest rib spacing ($\Delta/d = 0.267$), should be discarded due to, as previously discussed, they are sensitive to the incoming flow angle. Assuming that this is the case, they would probably therefore be bad engineering solutions. By discarding these, $C_{D,\text{avg}}$ will vary from 0.7 to 0.95. This means that adding any of these textiles (except S_C, h_2, Δ_{10}) would reduce drag significantly. The textiles with the lowest $C_{D,\text{avg}}$ in this area are $S_A, h_1, \Delta_{2.5}$ (0.70), S_A, h_1, Δ_{10} (0.72) and S_A, h_1, Δ_5 (0.73). This means that by choosing $S_A, h_1, \Delta_{2.5}$ on the cylinder surface rather than having a smooth cylinder, gives an average drag reduction of approximately 22.6%. Alongside giving a drag reduction compared to the smooth cylinder, these textiles also have noticeably lower $C_{D,\text{avg}}$ than the textiles without ribs, S_A, h_0 (0.89), S_B, h_0 (0.84), S_C, h_0 (0.78). So, choosing the ribbed textile $S_A, h_1, \Delta_{2.5}$ instead of S_C, h_0 gives an average drag reduction of 9.6%.

The Re in figure 4.1 is quite wide and it is reasonable to think that engineers are also interested in the $C_{D,\text{avg}}$ of narrower domains. This has been done in figure 4.2, where the domain has been split into two ranges. For the Re range $20000 < Re < 90000$, as shown in figure 4.2a, the three textiles with the lowest $C_{D,\text{avg}}$ are S_A, h_1, Δ_{10} (0.72), S_A, h_2, Δ_5 (0.73) and S_A, h_1, Δ_5 (0.74). This can be compared to the smooth cylinder (0.96) and the textiles without ribs, S_A, h_0 (0.94), S_B, h_0 (0.96) and S_C, h_0 (0.80). That means that choosing S_A, h_1, Δ_{10} instead of either a smooth surface, S_A, h_0, S_B, h_0 or S_C, h_0, yields savings in drag of 25.1%, 23.4%, 25.0% and 10.0%, respectively.

Furthermore, looking at figure 4.2b and the second half of the Re range ($90000 < Re < 160000$), yields the lowest $C_{D,\text{avg}}$ for textiles $S_B, h_{0.5}, \Delta_{10}$ (0.54), $S_A, h_{0.5}, \Delta_{10}$ (0.54) and $S_A, h_1, \Delta_{2.5}$ (0.56). The textiles with no ribs gave values for S_A, h_0 (0.84), S_B, h_0 (0.71) and S_C, h_0 (0.76). By choosing $S_B, h_{0.5}, \Delta_{10}$ or $S_B, h_{0.5}, \Delta_{10}$ in this region rather than a smooth surface and these textiles without ribs, give reductions in drag of 38.1% (smooth), 35.7% (S_A, h_0), 23.9% (S_B, h_0) and 29.0% (S_C, h_0).

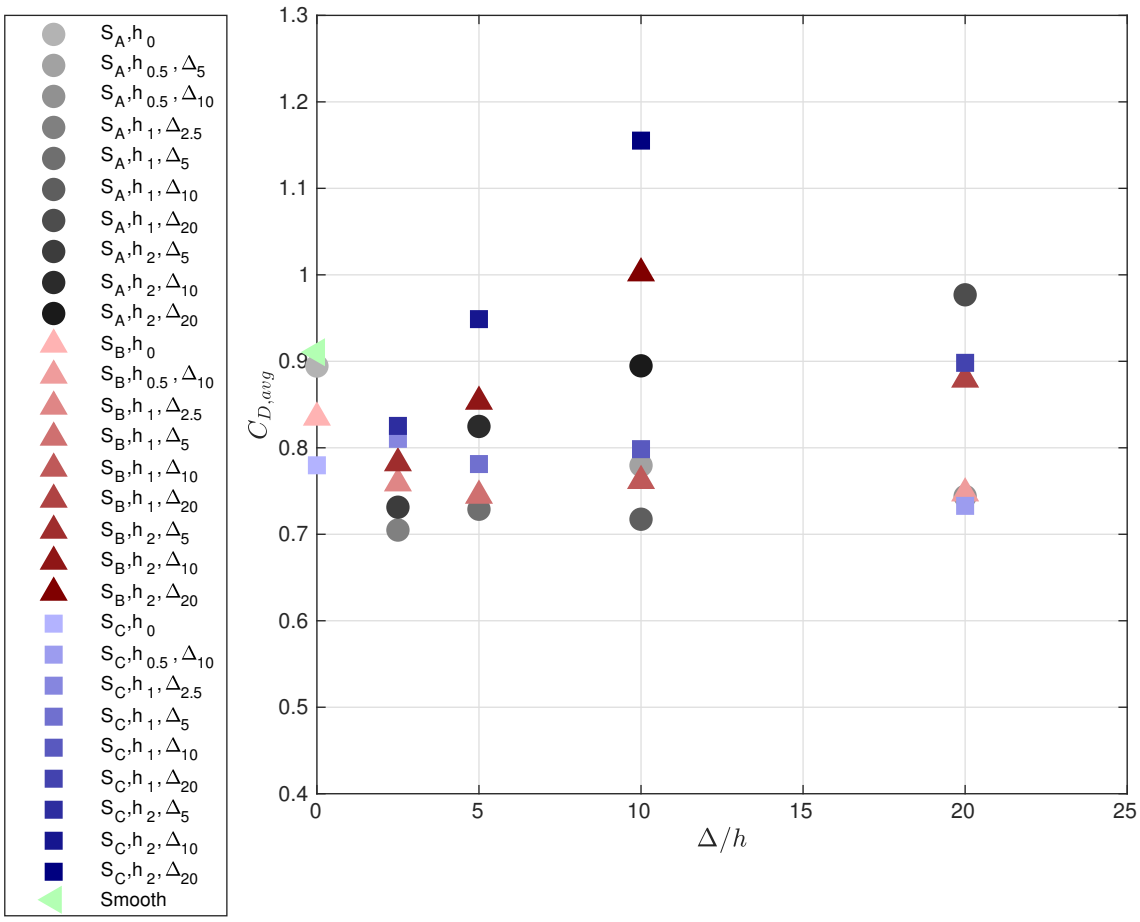

Figure 4.1: Average C_D across the measured Re range ($20000 < Re < 160000$).

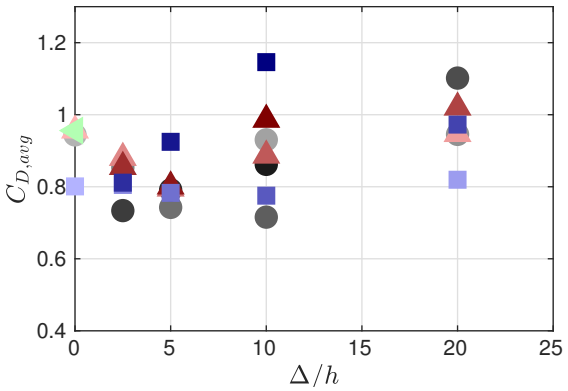

(a) Average C_D for the lower half of the Re-domain ($20000 < Re < 90000$).

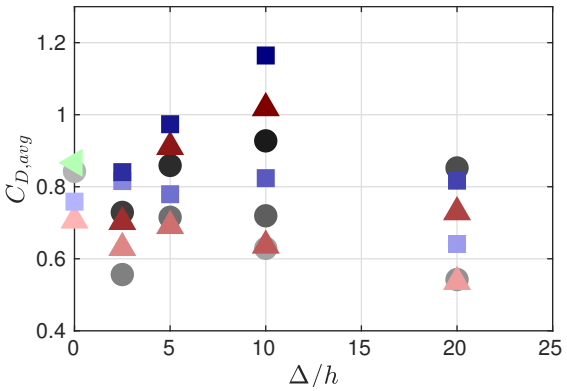

(b) Average C_D for the larger half of the Re-domain ($90000 < Re < 160000$).

Figure 4.2: Average C_D across halves of the measured Re-domain.

4.2 Minimum drag coefficient

The minimum drag coefficient for each textile, $C_{D,m}$, can also be plotted versus the relative rib spacing, Δ/h, as done in figure 4.3. The textiles without ribs have been plotted as having $\Delta/h = 0$. Some of the textiles have not been plotted due to their drag crisis being outside of the measured Re range. Looking at the remaining textiles, S_B, h_0 yields the lowest $C_{D,m}$ of about 0.49. This is a textile without ribs, which indicates that ribs in general increases $C_{D,m}$. There are however some ribbed textiles that have nearly as low a value as S_B, h_0, and $S_A, h_{0.5}, \Delta_{10}$ has a $C_{D,m}$ of approximately 0.5. As the smooth cylinder case did not yield a value inside the Re range, there is no base case value to compare with but generally it is known that it occurs at a much higher Re. However, a value of 0.5 is much larger than the smooth cylinder-value of 0.2, measured by Schewe [3]. This strengthens the belief that it is unlikely that the $C_{D,m}$ of a smooth cylinder can be replicated at lower Re.

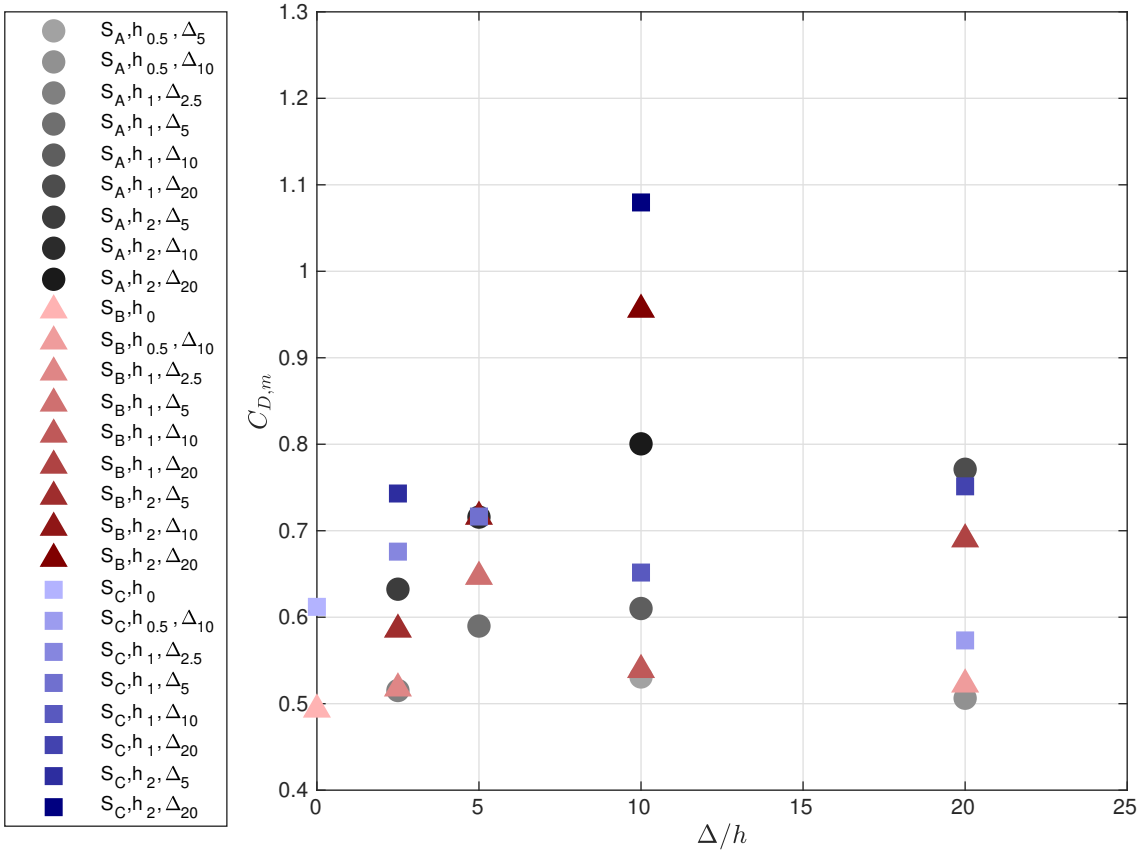

Figure 4.3: Minimum drag coefficient for all textiles plotted vs Δ/h.

Furthermore, it is again clear that textiles with $h/d = 0.0267$ and $\Delta/d = 0.267$ give large drag forces and are bad engineering choices. S_C, h_2, Δ_{20} even give a $C_{D,m}$ which are close to its $C_{D,s}$. This raises the question for this textile: what would happen if Δ/h was further increased to 20? Would $C_{D,m}$ increase again and give higher values than $C_{D,s}$, or would it start to decrease? A decreased value would indicate that $C_{D,m}$ can not become larger than $C_{D,s}$, yielding a maximum value for $C_{D,m}$. This has not been investigated in this work, but it is likely that the latter would be the case. At some point $C_{D,m}$ would have to start decreasing and decrease towards a value for a cylinder of equivalent surface micro-structure, as $\Delta/h \to \infty$. But again, as previously discussed, these cases would not be interesting due to their dependence on incoming flow angle.

4.3 Critical Reynolds number

The same type of analysis can be performed for Re_c, as illustrated in figure 4.4. The lowest Re_c in this figure is approximately 25,000 for $\Delta/h = 5$ and textile S_A, h_2, Δ_{10}. However, S_C, h_2, Δ_{10} was not plotted due to its Re_c being below 20,000 and not measured. Including this information helps further strengthening the trend with a distinct minimum peak in figure 4.4, as $\Delta/h = 5$ for S_C, h_2, Δ_{10} as well. This relative spacing also gives the smallest spread between each textile.

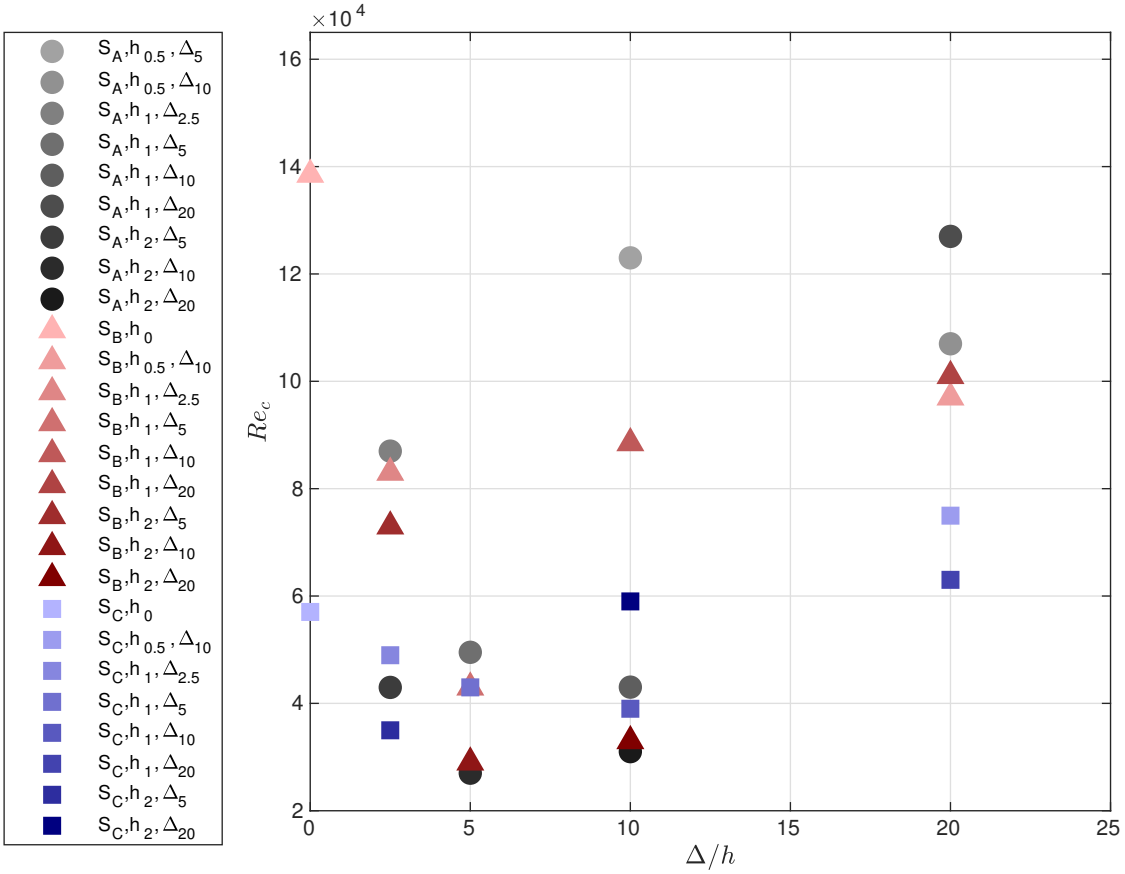

Figure 4.4: Critical Reynolds number for all textiles plotted vs their respective relative rib spacing, Δ/h.

If one were to draw a line between the points of smallest Re_c (or even the mean value) at each Δ/h, one would see a line that looks something like a parabola, with a global minimum at $\Delta/h = 5$ and increasing Re_c for both increasing and decreasing Δ/h. For increasing Δ/h above 10 though, the line might start to flatten somewhat, indicating a more logarithmic tendency in this area. This means that what was previously indicated in the discussion about the effect of varying the rib spacing, where there seemed to be an "optimal" rib spacing which would cause the lowest Re_c, seem to be correct. Based on these results, the optimal relative rib spacing is $\Delta/h = 5$.

Chapter 5

Model/Theory development

Thus far, the surface structures of the textiles have been parameterized using three design parameters: coating fabric (A, B and C), relative rib height (0.0067, 0.0133 and 0.0267) and relative rib spacing (2.5, 5, 10 and 20). However, these parameters do not fully illustrate the differences between the textiles in a rigorous way. For instance, the coating fabric parameter does not tell us anything about the actual surface structure, only that the micro-roughness is different from the other two cases. This leads to the question: is there a single non-dimensional parameter that could explain all ribbed surface structures, or maybe even all surface structures? By using surface parameters extracted from the surface spectra, one can try to plot the aerodynamic properties extracted from the C_D-Re curves versus the surface parameter for all textiles. The peaks from the spectra were, for each textile, placed in different groups based on their amplitude and orientation of frequency. The peak with maximum amplitude corresponds to the spanwise ribs at a frequency of 1 divided by the rib spacing, in the streamwise orientation. Peaks with amplitude above a certain percentage, Φ_1, of the maximum amplitude and frequency oriented in the streamwise direction, were used in calculating a streamwise macro parameter,

$$\mathcal{S}_1 = \frac{1}{n_1}\sum_{i=1}^{n_1}\frac{\phi_s(f_i)^2 f_i}{d}, \tag{5.1}$$

where n_1 is the number of streamwise macro-peaks, $\phi_s(f_i)$ is the peak amplitude, f_i the peak frequency, and d the cylinder diameter. A macro-peak is indicated by a green circle in figure 5.1, where it is only one peak that exceeds Φ_1, indicated by the green dashed line. Peaks with amplitude below Φ_1 but above a minimum value, Φ_0, where one below is assuming that the roughness peaks have negligible effects, and which also has streamwise oriented frequency, were used for calculation of a streamwise micro parameter,

$$\mathcal{S}_2 = \frac{1}{n_2}\sum_{j=1}^{n_2}\frac{\phi_s(f_j)^2 f_j}{d}. \tag{5.2}$$

These peaks are indicated by red circles in figure 5.1 as they have ϕ_s above Φ_0 (red dash-dotted line) and below Φ_1 (green dashed line). The same was done for peaks with amplitude above Φ_0 and frequency oriented perpendicular to the flow direction, giving the parameter

$$\mathcal{S}_3 = \frac{1}{n_3}\sum_{k=1}^{n_3}\frac{\phi_s(f_k)^2 f_k}{d}. \tag{5.3}$$

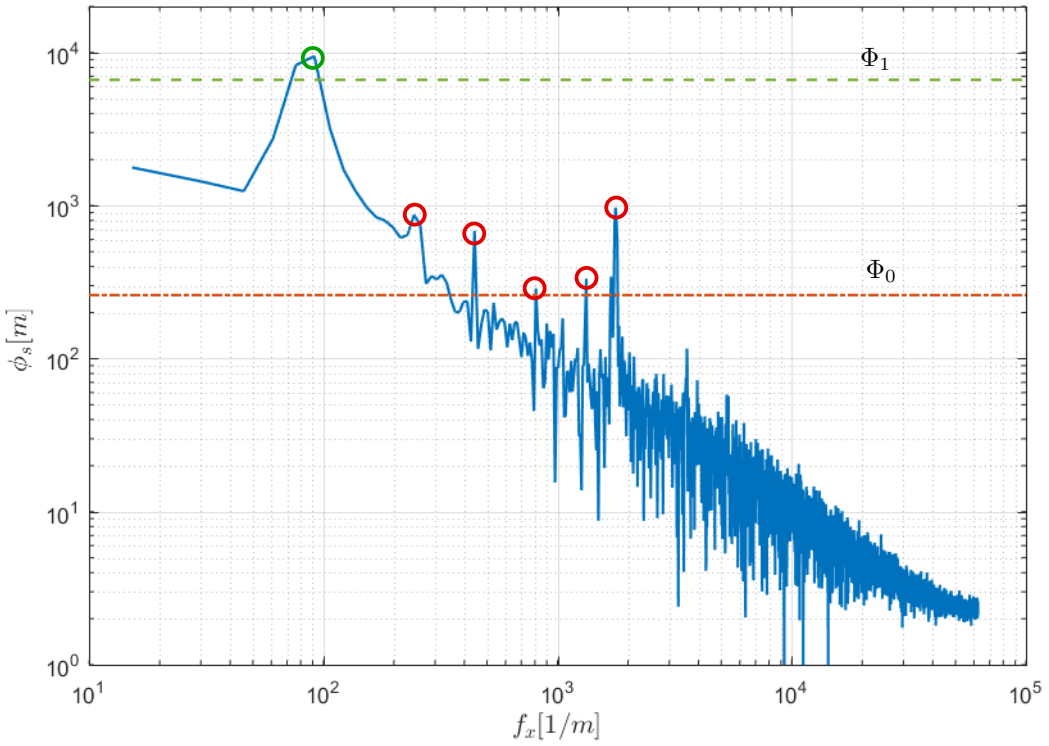

Figure 5.1: A logarithmic plot of the streamwise direction for the 2D FFT of surface S_C, h_1, Δ_{10}. Φ_1 and Φ_0 are indicated by the green dashed line and the red dash-dotted line, respectively. The macro peaks can then be found to be the peaks above Φ_1 indicated by green circles, and the micro-peaks between Φ_0 and Φ_1 indicated by red circles, which in turn are used to calculate $\mathcal{S}_1$ and $\mathcal{S}_2$.

And also for the rest of the peaks having an orientation of the frequency at some angle to the streamwise direction, giving

$$\mathcal{S}_4 = \frac{1}{n_4} \sum_{m=1}^{n_4} \frac{\phi_s(f_m)^2 f_m}{d}. \tag{5.4}$$

To get one surface parameter for each textile, these four parameters were multiplied by coefficients, summed and normalised, giving the surface parameter

$$\mathcal{S} = \frac{\mathcal{S}_1 + \zeta_2\mathcal{S}_2 + \zeta_3\mathcal{S}_3 + \zeta_4\mathcal{S}_4}{\zeta_2\zeta_3\zeta_4}, \tag{5.5}$$

where ζ_2, ζ_3 and ζ_4 are chosen coefficients. The coefficient for $\mathcal{S}_1$ are set to 1, giving coefficients that amplifies parameters $\mathcal{S}_2$, $\mathcal{S}_3$ and $\mathcal{S}_4$ based on their importance relative to the magnitude of $\mathcal{S}_1$. If the importance of $\mathcal{S}_1$ becomes small, then ζ_2, ζ_3 and ζ_4 would increase to large values. To prevent that $\mathcal{S} \to \infty$ when the importance of the macro-structure becomes 0, the coefficients are normalised by $\zeta_2\zeta_3\zeta_4$ yielding the coefficient for $\mathcal{S}_1$ to become $\frac{1}{\zeta_2\zeta_3\zeta_4}$. This means that the surface parameter becomes a function of five parameters, $\mathcal{S} = f(\Phi_1, \Phi_0, \zeta_2, \zeta_3, \zeta_4)$. By testing, and combining a wide range of these parameters, and plotting the textiles Re_c and $C_{D,m}$ versus the resulting $\mathcal{S}$, one can plot different polynomial fits and calculate their respective standard deviations, σ. The parameters used for calculating the $\mathcal{S}$ that gives the polynomial fit with the lowest σ, would be the parameters for $\mathcal{S}$ that models Re_c and $C_{D,m}$ the best way.

As previously shown and discussed, the aerodynamic properties retrieved from the C_D-Re curve (such as Re_c, $C_{D,m}$, $C_{D,t}$ etc.) are affected differently when varying the rib geometry and the micro-roughness. Some properties were largely dependent on the rib height, some on the rib spacing and some on the choice of coating fabric. This would indicate that different parameters should be chosen for $\mathcal{S}$ when being correlated to different aerodynamic properties. The relative magnitude of the different coefficients would tell what features of the surface topology that are the most important for a given aerodynamic property. Low values for ζ_2, ζ_3 and ζ_4 would then indicate a larger dependency on the macro parameter, compared to what the magnitude of $\mathcal{S}_1$ relative to the magnitude of the other three parameters would otherwise indicate, meaning that the streamwise macro roughness would be the driving parameter. Likewise, a relatively large ζ_2 would indicate larger dependency on the streamwise micro parameter, a relatively large ζ_3 would indicate larger dependency on the roughness perpendicular to the flow and a relatively large ζ_4 would indicate larger dependency on the roughness with some angle to the flow. Different surface parameters have therefore been made in figures 5.2a and 5.2b for Re_c and $C_{D,m}$, respectively, giving $\mathcal{S}_a$ for Re_c and $\mathcal{S}_b$ for $C_{D,m}$.

For calculations of $\mathcal{S}_a$, the following parameter values were used: $\Phi_1 = 0.2$, $\Phi_0 = 500$, $\zeta_2 = 25$, $\zeta_3 = 1200$ and $\zeta_4 = 20$. This means that for Re_c, the streamwise micro roughness has an effect relative to $\mathcal{S}_1$ which is 25 times the magnitude of $\mathcal{S}_2$. Further on, the perpendicular roughness has an effect relative to $\mathcal{S}_1$ which is 1200 times the magnitude of $\mathcal{S}_3$. This is the biggest coefficient of the three, probably due to S_3 being very small, but it would also mean that the roughness of smallest scale has larger effect being in the perpendicular direction than in the streamwise direction. Looking at the results in figure 5.2a, the polynomial fit is a 2nd degree curve giving $\sigma = 15,770$. This is a relatively large standard deviation (over 10% of the max value) and does not indicate that the optimal model has been found. Also, the point of $\mathcal{S}_a = 0$ does not replicate Re_c for a smooth cylinder which should be close to 300,000. The polynomial fit gives a value of 111,390. The reason for this might be the lack of test cases with $140,000 < Re < 300,000$. The shape of the curve is, however, as expected since it has some equality to what was found when plotted versus Δ/h.

Moving on to $C_{D,m}$, things look a bit better. Here, $\Phi_1 = 0.7$, $\Phi_0 = 260$, $\zeta_2 = 500$, $\zeta_3 = 91,000$ and $\zeta_4 = 700$, were used in calculating $\mathcal{S}_b$. These coefficients are between 20 and 80 times what

they were for Re_c, which means that the streamwise macro roughness has lower effect on $C_{D,m}$ than Re_c compared to the effects of the micro roughness in the streamwise, perpendicular and angled directions. The micro roughness is therefore the driving parameter in deciding $C_{D,m}$, and adding micro roughness scales would affect the $C_{D,m}$ in a larger magnitude than adding macro roughness scales. ζ_3 is also here the largest coefficient by approximately a factor of 100, which again probably is due to very low $\mathcal{S}_3$, but also show the importance of small-scale roughness in the perpendicular orientation. The polynomial fit for $C_{D,m}$ is a 2nd degree curve with $\sigma = 0.0437$ which is within 4-9% of the measured values. This curve suggests that for a perfectly smooth cylinder ($\mathcal{S}_b = 0$), $C_{D,m}$ becomes 0.52. This is wrong, as Schewe [3] has shown it to be around 0.2. But again, the test cases in this work do not cover the range down towards the smooth cylinder. Further on, increasing $\mathcal{S}_b$ increases $C_{D,m}$ with a decreasing slope until it flattens out around a $C_{D,m}$ of 1.2. This is consistent to what was discussed when looking at the global results, i.e., there is a maximum theoretical $C_{D,m}$ and that this value might be equal to $C_{D,s}$. The plotted curve therefore makes sense as it increases in some polynomial way before it starts to converge towards 1.2 for large $\mathcal{S}_b$.

The method used in this work is only one of many potentially interesting methods to define surface structures using the surface spectrum. A larger study of these methods is needed to determine whether the employed method is one of the better ones. Also, data-points from a larger Re range would also improve the results. What can be said about the retrieved results is that the two models created can be used in the measured Re range to calculate Re_c with a relatively large error, and $C_{D,m}$ with an expected error within $\pm$ 9%. Also, for an engineer who designs surface structures for minimum drag at minimum speeds, by using this model the optimal surface structure would have parameters $\mathcal{S}_a = 5 \cdot 10^8$ and $\mathcal{S}_b$ as small as possible.

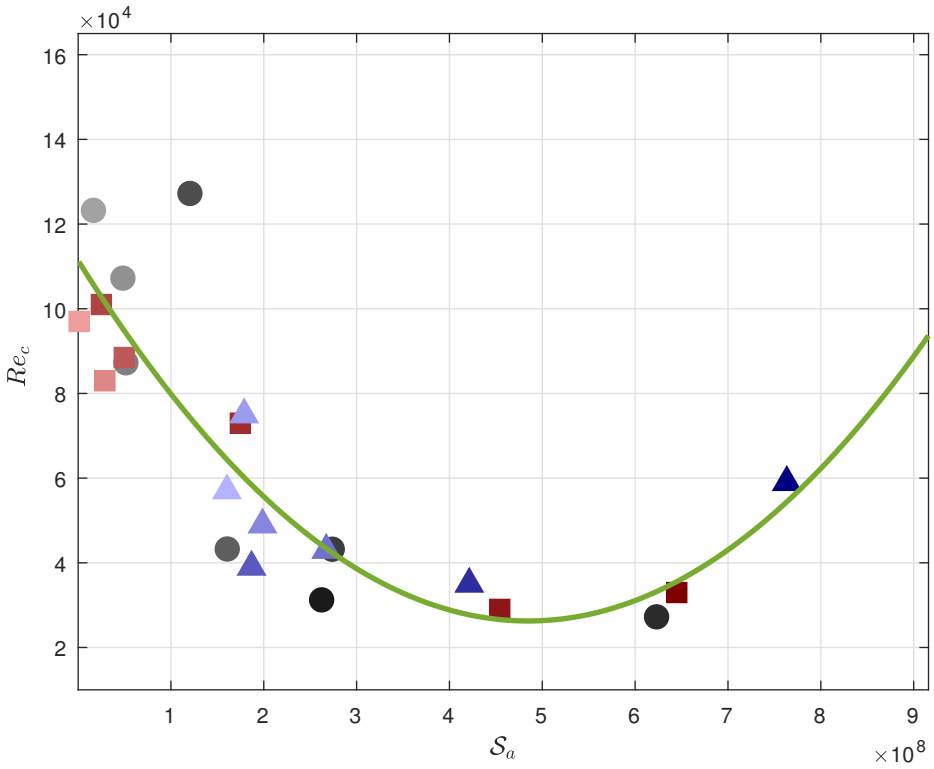

(a) Critical Reynolds number vs the surface parameter, with a 2nd degree polynomial fit ($111,390 - 3.51 \cdot 10^{-4}\mathcal{S}_a + 3.62 \cdot 10^{-13}\mathcal{S}_a^2$) and $\sigma = 15770$.

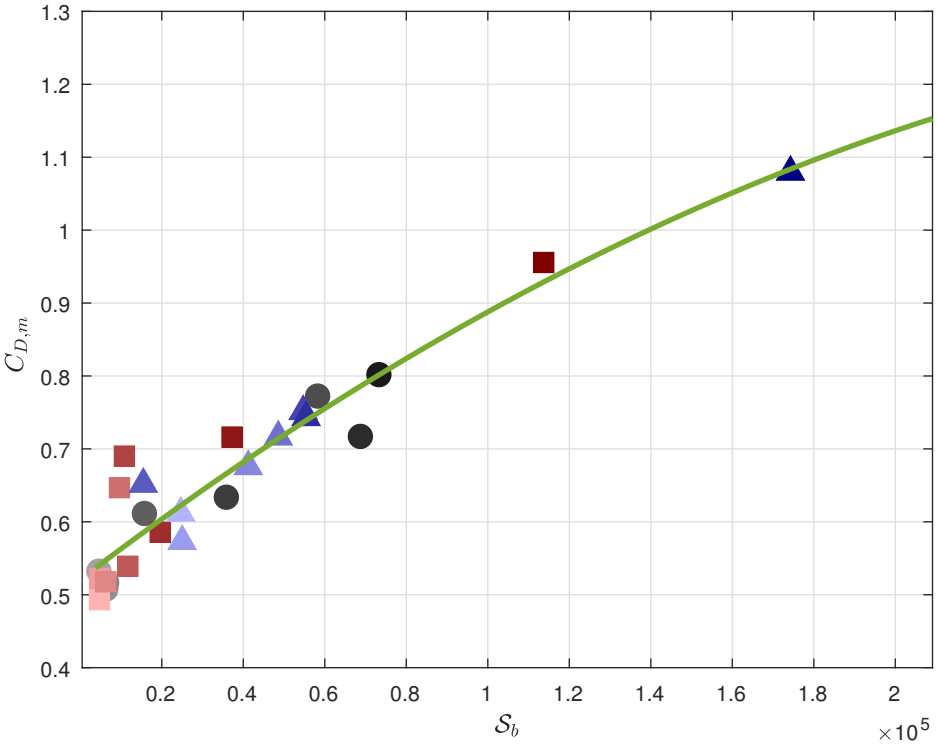

(b) Minimum drag coefficient vs the surface parameter, with a 2nd degree polynomial fit ($0.52 + 4.26 \cdot 10^{-6}\mathcal{S}_b - 5.93 \cdot 10^{-12}\mathcal{S}_b^2$) and $\sigma = 0.0437$.

Figure 5.2: The best polynomial fits found for variations of the parameters in $\mathcal{S}$.

Chapter 6

Conclusions

The measurements performed and analysed in this work showed that adding spanwise ribs to the surface of a cylinder with a given micro-roughness, could decrease both the instantaneous C_D and the $C_{D,\text{avg}}$ at any partition of the measured Re range investigated here. This is due to the effect the ribs have on the trajectory of the C_D-Re curve and the point of $C_{D,m}$, $C_{D,s}$, the critical slope, the Re_c, the $C_{D,m}$, the supercritical slope and the $C_{D,t}$. The effect of the ribs on these properties was dependent on the rib size, the rib spacing and the micro-roughness. Increasing the rib size yielded higher $C_{D,s}$, $C_{D,m}$ and $C_{D,t}$, and a decreasing Re_c. It had no effect on the critical and supercritical slope, but decreased the value of the St peak at Re_c, meaning decrease in the frequency of the vortex shedding. The rib spacing had a different effect. An optimal rib spacing of $\Delta/h = 5$ caused the lowest Re_c, and from this point either increasing or decreasing the rib spacing caused an increasing Re_c. The smallest rib spacing gave the lowest $C_{D,m}$ and by increasing the rib spacing, the $C_{D,m}$ was increased. For the largest rib spacing, the drag seemed to become dependent on the actual position of the ribs relative to the incoming flow, rather than the spacing between them. A rib spacing larger than $\Delta/d = 0.133$, would therefore not be a good choice based on the measurements done during this work. When micro-roughness was added at increasing levels to the ribbed cylinder, the general trend showed that the Re_c decreased, $C_{D,m}$ increased, the supercritical slope became steeper and $C_{D,t}$ increased. This is consistent with what was expected, as one would expect that a larger micro-roughness would increase the skin friction when the boundary layer becomes turbulent.

By taking the average of C_D throughout the measured Re range ($20,000 < Re < 160,000$), the average drag savings by choosing ribbed surface textiles instead of a smooth surface, was found. The maximum savings in average drag was found to be 22.6% for choosing textile $S_A, h_1, \Delta_{2.5}$. The same was done for the two halves of the Re range. For the lowest Re half ($20,000 < Re < 90,000$), choosing textile S_A, h_1, Δ_{10} gave an average drag reduction of 25.1%. For the second half ($90,000 < Re < 160,000$), $S_B, h_{0.5}, \Delta_{10}$ and $S_A, h_{0.5}, \Delta_{10}$ gave average drag reductions of 38.1%.

The $C_{D,m}$ for all textiles varied between approximately 0.5 and 1.1. S_B, h_0 gave the smallest $C_{D,m}$ while S_C, h_2, Δ_{20} gave the largest. The textiles with $\Delta/d = 0.267$ gave generally bad results. These textiles seemed to be very dependent on the incoming flow angle, and were therefore discarded as possible engineering solutions. The global results for Re_c unveiled that $\Delta/h = 5$ was the best choice of relative spacing for decreasing Re_c. The Re_c for the tested cases varied all the way outside of the measured Re range. S_C, h_2, Δ_{10} gave the lowest value just below 20,000, while S_A, h_0 and the smooth cylinder gave values above 160,000.

Models for Re_c and $C_{D,m}$ within the measured Re range was made by extracting parameters for each textile from their respective surface spectra. The models found global trends where Re_c and

$C_{D,m}$ were dependent on the chosen parameters, with a significant error for Re_c and an expected error of $\pm$ 9% for $C_{D,m}$.

Considering all facets investigated herein, for the investigated Re range, $S_A, h_1, \Delta_{2.5}$ would be the best suited for applications because it produced the minimum drag over the tested range.

Bibliography

[1] Yunus A. Cengel and John M. Cimbala. *Fluid Mechanics: Fundamentals and Applications, 3rd ed.* The McGraw-Hill Companies, 2014.

[2] Luca Oggiano, Len Brownlie, Olga Troynikov, Lars Morten Bardal, Camilla Sæter, and Lars Sætran. A review on skin suits and sport garment aerodynamics: guidelines and state of the art. *Procedia Engineering*, 60:91–98, 2013.

[3] Günter Schewe. Reynolds-number effects in flow around more-or-less bluff bodies. *Journal of Wind Engineering and Industrial Aerodynamics*, 89(14-15):1267–1289, 2001.

[4] Elmar Achenbach. Influence of surface roughness on the cross-flow around a circular cylinder. *Journal of Fluid Mechanics*, 46(2):321–335, 1971.

[5] PW Bearman and JK Harvey. Control of circular cylinder flow by the use of dimples. *AIAA Journal*, 31(10):1753–1756, 1993.

[6] Leonard William Brownlie. *Aerodynamic characteristics of sports apparel*. PhD thesis, Theses (School of Kinesiology)/Simon Fraser University, 1992.

[7] Hee-Chang Lim and Sang-Joon Lee. Flow control of circular cylinders with longitudinal grooved surfaces. *AIAA Journal*, 40(10):2027–2036, 2002.

[8] Shabnam Raayai-Ardakani and Gareth H McKinley. Drag reduction using wrinkled surfaces in high Reynolds number laminar boundary layer flows. *Physics of Fluids*, 29(9):093605, 2017.

[9] MJ Walsh and LM Weinstein. Drag and heat-transfer characteristics of small longitudinally ribbed surfaces. *AIAA Journal*, 17(7):770–771, 1979.

[10] NWM Ko, YC Leung, and JJJ Chen. Flow past v-groove circular cylinders. *AIAA Journal*, 25(6):806–811, 1987.

[11] Yo Nakamura and Y Tomonari. The effects of surface roughness on the flow past circular cylinders at high Reynolds numbers. *Journal of Fluid Mechanics*, 123:363–378, 1982.

[12] Takeyoshi Kimura and Michihisa Tsutahara. Fluid dynamic effects of grooves on circular cylinder surface. *AIAA Journal*, 29(12):2062–2068, 1991.

[13] Yoichi Yamagishi and Makoto Oki. Effect of groove shape on flow characteristics around a circular cylinder with grooves. *Journal of Visualization*, 7(3):209–216, 2004.

[14] Yoichi Yamagishi and Makoto Oki. Effect of the number of grooves on flow characteristics around a circular cylinder with triangular grooves. *Journal of Visualization*, 8(1):57–64, 2005.

[15] Anwar Ahmed and Byram Bays-Muchmore. Transverse flow over a wavy cylinder. *Physics of Fluids A: Fluid Dynamics*, 4(9):1959–1967, 1992.

[16] K Lam and YF Lin. Effects of wavelength and amplitude of a wavy cylinder in cross-flow at low Reynolds numbers. *Journal of Fluid Mechanics*, 620:195–220, 2009.

[17] T Zhou, SF Mohd Razali, Z Hao, and L Cheng. On the study of vortex-induced vibration of a cylinder with helical strakes. *Journal of Fluids and Structures*, 27(7):903–917, 2011.

[18] Sang-Joon Lee and Hyoung-Bum Kim. The effect of surface protrusions on the near wake of a circular cylinder. *Journal of Wind Engineering and Industrial Aerodynamics*, 69:351–361, 1997.

[19] Jong-Yeon Hwang and Kyung-Soo Yang. Drag reduction on a circular cylinder using dual detached splitter plates. *Journal of Wind Engineering and Industrial Aerodynamics*, 95(7):551–564, 2007.

[20] Kai Zhang, Hiroshi Katsuchi, Dai Zhou, Hitoshi Yamada, and Zhaolong Han. Numerical study on the effect of shape modification to the flow around circular cylinders. *Journal of Wind Engineering and Industrial Aerodynamics*, 152:23–40, 2016.

[21] Toshio Matsumura, Toshiki Yura, Naoshi Kikuchi, Tetsuo Matsumoto, Hitoshi Takeuchi, Kunio Iwasaki, and Yasuhiro Tominaga. Development of low wind-pressure insulated wires. *Furukawa Electric Review*, pages 39–44, 2002.

[22] MM Zdravkovich. Review and classification of various aerodynamic and hydrodynamic means for suppressing vortex shedding. *Journal of Wind Engineering and Industrial Aerodynamics*, 7(2):145–189, 1981.

[23] Anatol Roshko. Experiments on the flow past a circular cylinder at very high Reynolds number. *Journal of Fluid Mechanics*, 10(3):345–356, 1961.

[24] Marcus Hultmark and Alexander J Smits. Temperature corrections for constant temperature and constant current hot-wire anemometers. *Measurement Science and Technology*, 21(10):105404, 2010.

Appendix

Textiles

Table 6.1: Test cases and properties.

Textile	Coating fabric	h/d	Δ/h	Number of ribs	θ_1 [deg]	$\mathcal{S}_a$	$\mathcal{S}_b$
S_A, h_0	A	0	-	0	-	1.459e07	4,749
$S_A, h_{0.5}, \Delta_5$	A	0.0067	10	35	157	1.762e07	4,806
$S_A, h_{0.5}, \Delta_{10}$	A	0.0067	20	19	152	4.939e07	6,508
$S_A, h_1, \Delta_{2.5}$	A	0.0133	2.5	46	156	5.261e07	6,692
S_A, h_1, Δ_5	A	0.0133	5	30	157	-	-
S_A, h_1, Δ_{10}	A	0.0133	10	18	157	16.17e07	15,985
S_A, h_1, Δ_{20}	A	0.0133	20	10	153	12.15e07	58,485
S_A, h_2, Δ_5	A	0.0267	2.5	23	154	27.48e07	36,091
S_A, h_2, Δ_{10}	A	0.0267	5	15	153	62.42e07	68,978
S_A, h_2, Δ_{20}	A	0.0267	10	9	150	26.34e07	73,524
S_B, h_0	B	0	-	0	-	-	4,701
$S_B, h_{0.5}, \Delta_{10}$	B	0.0067	20	19	152	0.115e07	4,736
$S_B, h_1, \Delta_{2.5}$	B	0.0133	2.5	46	156	2.893e07	6,288
S_B, h_1, Δ_5	B	0.0133	5	30	157	3.675e07	9,620
S_B, h_1, Δ_{10}	B	0.0133	10	18	157	4.976e07	11,681
S_B, h_1, Δ_{20}	B	0.0133	20	10	153	2.512e07	10,828
S_B, h_2, Δ_5	B	0.0267	2.5	23	154	17.48e07	19,612
S_B, h_2, Δ_{10}	B	0.0267	5	15	153	45.42e07	37,234
S_B, h_2, Δ_{20}	B	0.0267	10	9	150	64.49e07	113,720
S_C, h_0	C	0	-	0	-	16.04e07	24,660
$S_C, h_{0.5}, \Delta_{10}$	C	0.0067	20	19	152	17.89e07	25,000
$S_C, h_1, \Delta_{2.5}$	C	0.0133	2.5	46	156	19.86e07	41,210
S_C, h_1, Δ_5	C	0.0133	5	30	157	26.73e07	48,590
S_C, h_1, Δ_{10}	C	0.0133	10	18	157	18.69e07	15,470
S_C, h_1, Δ_{20}	C	0.0133	20	10	153	16.93e07	54,690
S_C, h_2, Δ_5	C	0.0267	2.5	23	154	42.13e07	55,420
S_C, h_2, Δ_{10}	C	0.0267	5	15	153	99.38e07	95,930
S_C, h_2, Δ_{20}	C	0.0267	10	9	150	76.33e07	174,260

Aerodynamic properties

Table 6.2: Aerodynamic properties for all textiles.

Textile name	$C_{D,s}$	Critical slope	Re_c	$C_{D,m}$	Supercritical slope	$C_{D,t}$
S_A, h_0	0.94	-	-	-	-	-
$S_A, h_{0.5}, \Delta_5$	0.98	-6.5e-06	123,000	0.53	1.0e-06	-
$S_A, h_{0.5}, \Delta_{10}$	1.03	-9.3e-06	107,000	0.51	1.0e-06	-
$S_A, h_1, \Delta_{2.5}$	0.97	-1.5e-05	87,000	0.52	1.5e-06	0.60
S_A, h_1, Δ_5	1.00	-2.1e-05	49,500	0.59	2.5e-06	0.73
S_A, h_1, Δ_{10}	1.09	-2.2e-05	43,000	0.61	2.0e-06	0.73
S_A, h_1, Δ_{20}	1.11	-6.5e-06	127,000	0.77	1.4e-06	-
S_A, h_2, Δ_5	1.07	-1.9e-05	43,000	0.63	2.1e-06	0.73
S_A, h_2, Δ_{10}	-	-2.9e-05	27,000	0.72	3.1e-06	0.86
S_A, h_2, Δ_{20}	-	-1.7e-05	31,000	0.80	4.0e-06	0.93
S_B, h_0	0.96	-8.9e-06	138,500	0.49	2.1e-06	-
$S_B, h_{0.5}, \Delta_{10}$	1.00	-1.3e-05	97,000	0.52	2.0e-07	-
$S_B, h_1, \Delta_{2.5}$	1.00	-1.5e-05	83,000	0.52	4.2e-06	0.69
S_B, h_1, Δ_5	1.05	-1.3e-05	-	0.65	1.2e-06	-
S_B, h_1, Δ_{10}	1.08	-1.0e-05	88,500	0.54	2.6e-06	-
S_B, h_1, Δ_{20}	1.14	-6.3e-06	101,000	0.69	1.9e-06	-
S_B, h_2, Δ_5	1.13	-1.4e-05	73,000	0.59	2.4e-06	-
S_B, h_2, Δ_{10}	-	-2.4e-05	29,000	0.72	-	0.93
S_B, h_2, Δ_{20}	-	-1.5e-05	33,000	0.96	1.3e-06	1.02
S_C, h_0	0.99	-1.6e-05	57,000	0.61	5.9e-06	0.75
$S_C, h_{0.5}, \Delta_{10}$	0.99	-1.2e-05	75,000	0.57	1.5e-06	-
$S_C, h_1, \Delta_{2.5}$	1.01	-1.6e-05	49,000	0.68	5.1e-06	0.81
S_C, h_1, Δ_5	-	-1.4e-05	43,000	0.72	9.5e-07	-
S_C, h_1, Δ_{10}	-	-2.4e-05	39,000	0.65	6.9e-06	0.82
S_C, h_1, Δ_{20}	1.13	-1.8e-05	-	0.75	1.9e-06	-
S_C, h_2, Δ_5	-	-2.2e-05	35,000	0.74	1.5e-06	0.85
S_C, h_2, Δ_{10}	-	-	< 20,000	-	5.0e-06	0.97
S_C, h_2, Δ_{20}	1.18	-4.8e-06	59,000	1.08	1.0e-05	1.16

Additional plots

Figures 6.1, 6.2, 6.3, 6.4, 6.5, 6.6, 6.7, 6.8 and 6.9 show effects on the C_D-Re curves and the St-numbers, by varying the surface coating, the relative rib spacing and the rib height. These figures show the same trends, with minor differences, as previously shown in sections 3.1, 3.2 and 3.3.

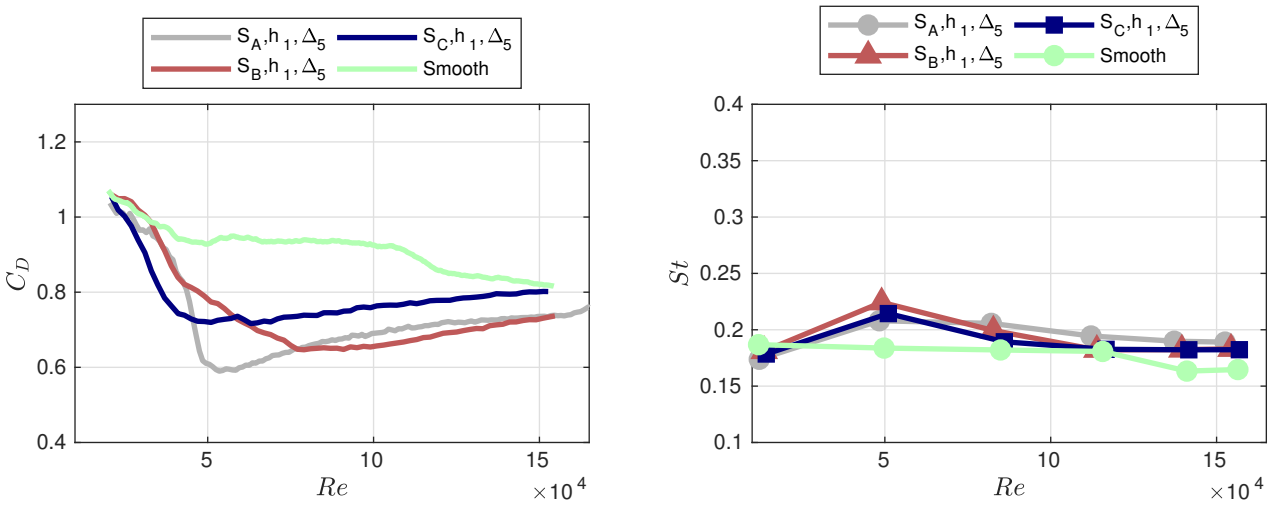

(a) Caption (b) Caption

Figure 6.1: Effect of varying the coating fabric for textiles with $h/d = 0.0133$ and Δ/h=5.

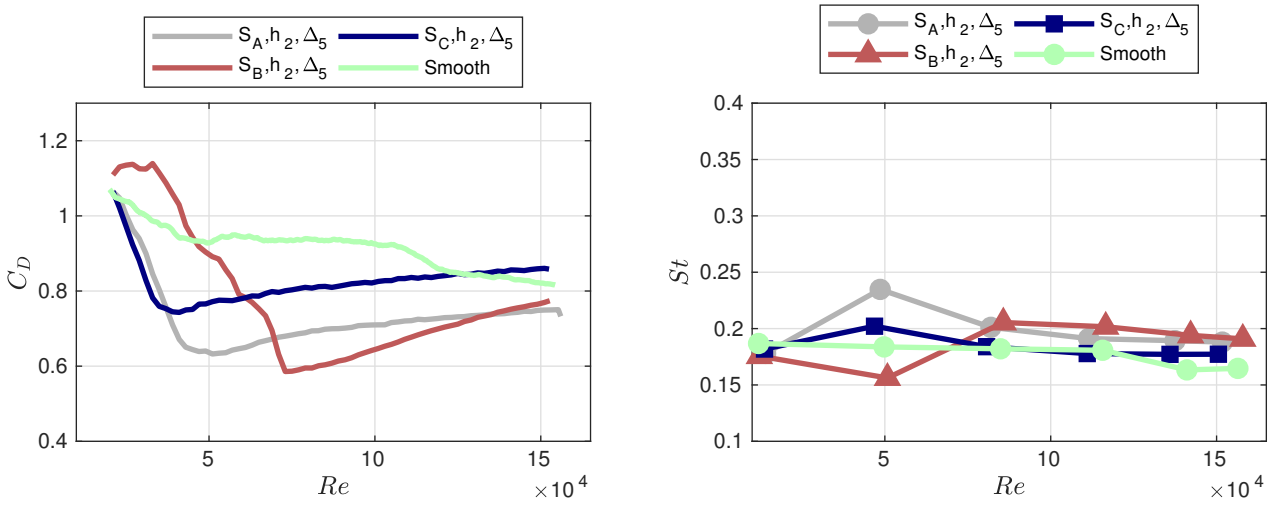

(a) Caption (b) Caption

Figure 6.2: Effect of varying the coating fabric for textiles with $h/D = 0.0133$ and Δ/h=10.

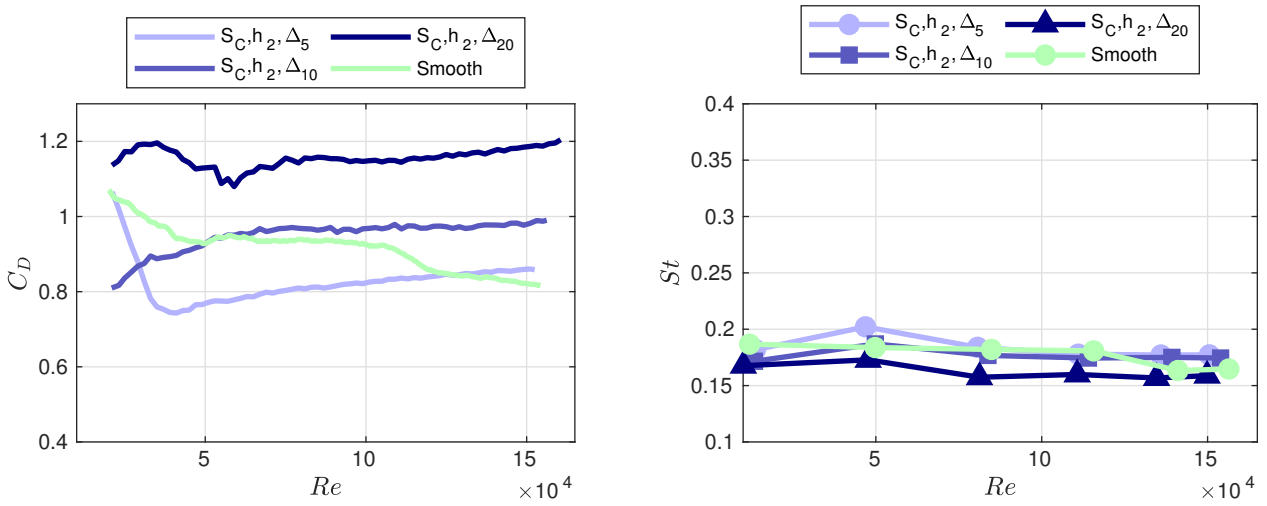

(a) (b)

Figure 6.3: Effect on C_D-Re curve by varying the rib spacing, for coating fabric C and $h/d = 0.0267$.

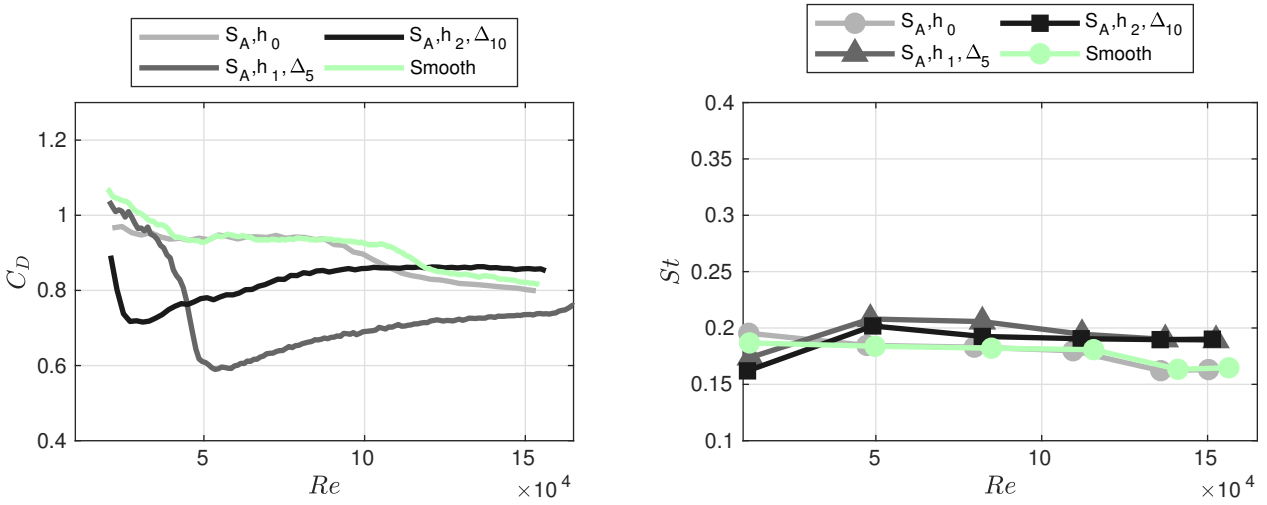

(a) Caption (b) Caption

Figure 6.4: Effect on C_D-Re curve by varying the rib size, for coating fabric A and relative rib spacing 5.

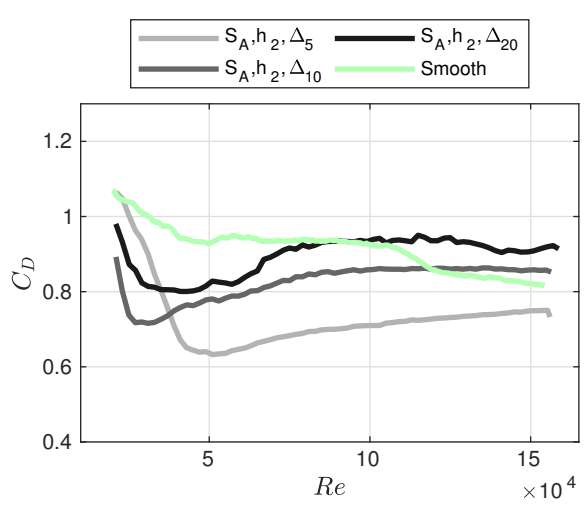

(a) C_D-Re

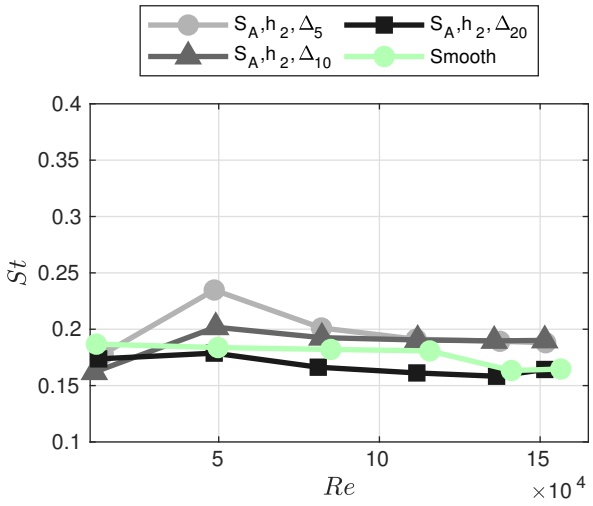

(b) St-Re

Figure 6.5: Effect on C_D-Re curve by varying the rib spacing, for coating fabric A and relative rib height $h/d = 0.0267$.

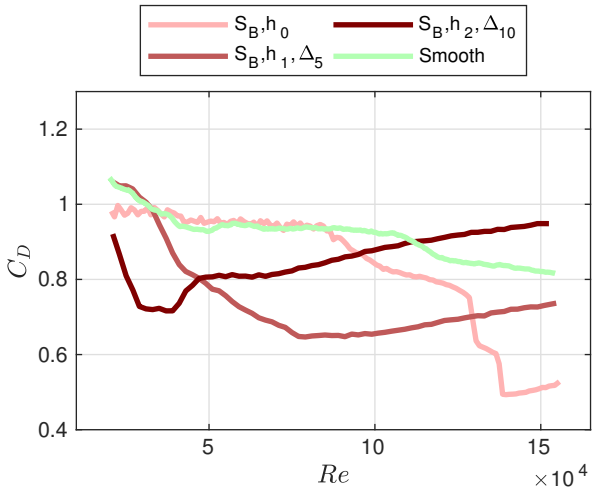

(a) C_D-Re

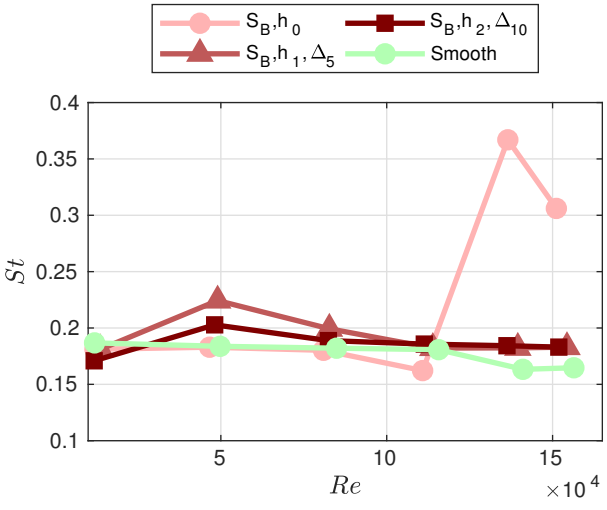

(b) St-Re

Figure 6.6: Effect on C_D-Re curve and St by varying the relative rib height, for coating fabric B and relative rib spacing 5.

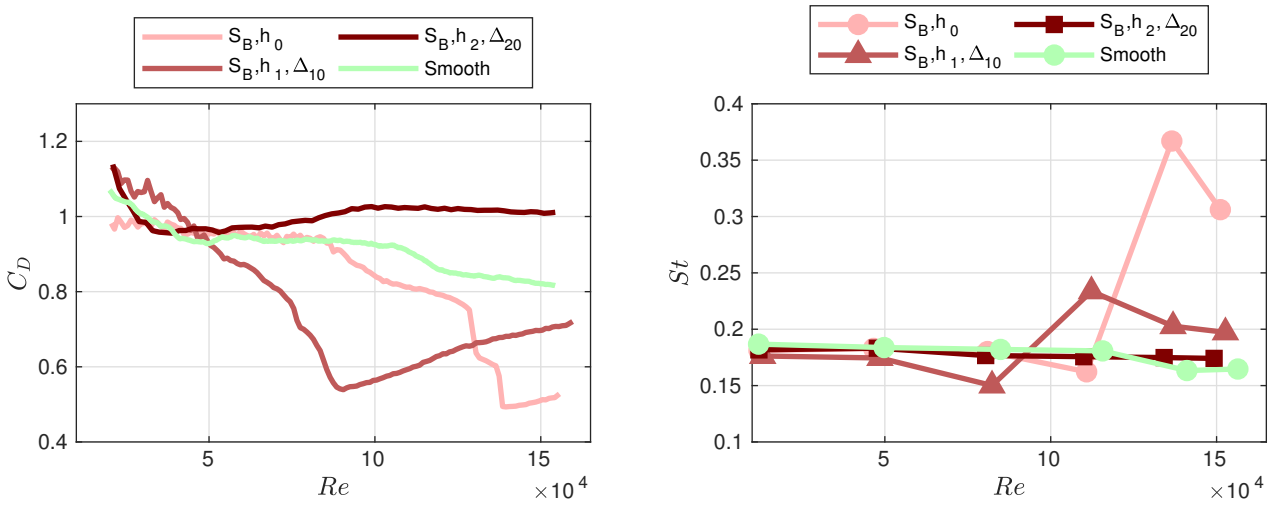

(a) C_D-Re (b) St-Re

Figure 6.7: Effect on C_D-Re curve and St by varying the relative rib height, for coating fabric B and relative rib spacing 10.

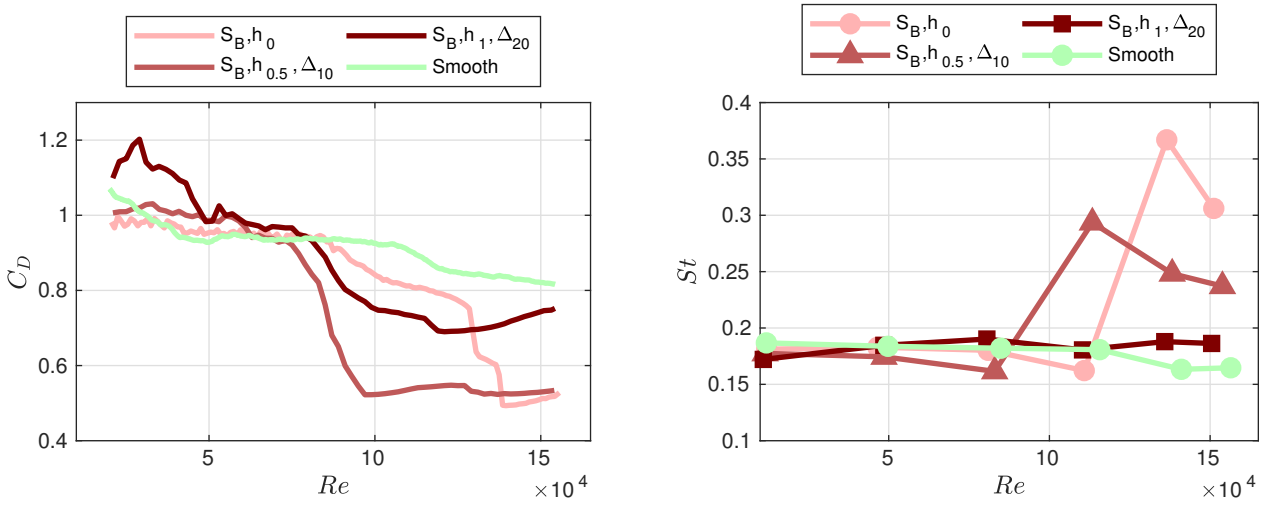

(a) C_D-Re (b) St-Re

Figure 6.8: Effect on C_D-Re curve and St by varying the relative rib height, for coating fabric B and relative rib spacing 20.

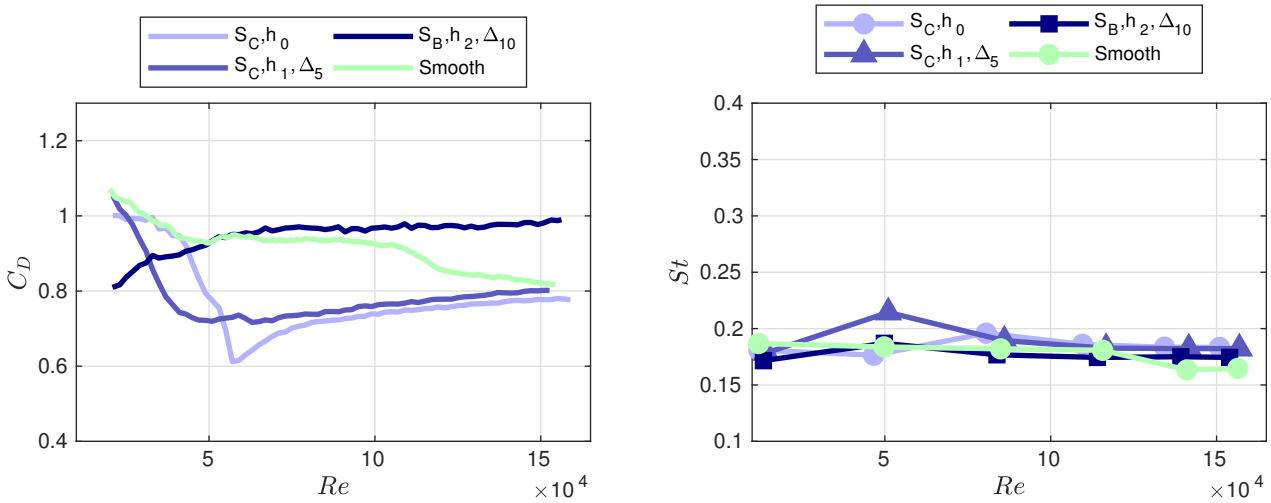

(a) C_D-Re (b) St-Re

Figure 6.9: Effect on C_D-Re curve and St by varying the relative rib height, for coating fabric C and relative rib spacing 5.